A RATIONAL DERIVATION OF A TUBE LAW FROM SHELL THEORY

by Robert J. Whittaker[1], Matthias Heil[2],
Oliver E. Jensen[3] & Sarah L. Waters[1]

([1] *Oxford Centre for Industrial and Applied Mathematics, University of Oxford, 24–29 St. Giles', Oxford, OX1 3LB, UK*
[2] *School of Mathematics, University of Manchester, Oxford Road, Manchester, M13 9PL, UK*
[3] *School of Mathematical Sciences, University of Nottingham, University Park, Nottingham, NG7 2RD, UK*)

Summary

We consider small-amplitude deformations of a long thin-walled elastic tube having an initially axially uniform elliptical cross section. The tube is subject to an axial pre-stress, and the deformations result from an applied transmural pressure. An approximate tube law (linking the transmural pressure, the cross-sectional area, and its axial derivatives) is derived from shell theory in the distinguished asymptotic limit in which the tube's behaviour is dominated by the restoring forces from the axial pre-stress and azimuthal bending. This is possible because the deformations of the tube induced by both the transmural pressure and the axial forces can be described, to very good approximation, by a single azimuthal mode of deformation of axially varying amplitude. The resulting tube law is compared with numerical solutions of the full shell equations and good agreement is found (provided the tube is sufficiently long and the wall not too thin so that in-plane shearing is negligible). We discuss the applications of our results to the modelling of flow in collapsible tubes.

1. Introduction

Fluid-filled elastic-walled tubes exist in many biological organisms, forming transport conduits for the circulatory, lymphatic and respiratory systems (1; 2). Mathematical modelling of these systems naturally requires consideration of the interaction between the mechanics of the internal fluid and those of the tube wall. In particular, it is important to know how the shape of the wall is affected by the stresses (mainly pressure in the case of relatively inviscid fluids) that the fluid exerts on the tube wall. Changes to the wall position alter the flow domain and displace fluid. Both effects can have a significant effect on the internal flow, leading to strong fluid–structure interaction.

Many theoretical studies of physiological flows in elastic vessels are based on spatially one-dimensional models of the fluid mechanics which describe the system in terms of the volume flux (or the average velocity u), the fluid pressure $p_{\rm int}$, and the vessel's cross-sectional area A, as functions of distance along the vessel and time. We refer to the papers by Sherwin *et al.* (3), Fullana and Zaleski (4), Elad *et al.* (5), and Berkouk *et al.* (6) for representative studies of flows in the arterial, venous, respiratory and cerebrospinal systems, respectively. Our own interest in the problem arises from studies of flow-induced self-excited oscillations in the Starling resistor. In the typical experimental setup, shown in Fig. 1, viscous fluid

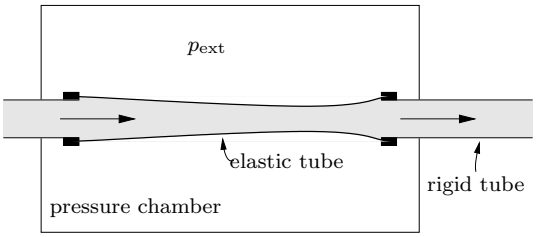

Fig. 1: *The experimental setup, known as a 'Starling resistor', which comprises an elastic tube clamped between two rigid pipes, surrounded by an outer pressure chamber. Flow can be driven along the interior of the tube and the external pressure p_{ext} in the surrounding chamber can be adjusted to control the degree of collapse of the elastic section.*

is driven through a thin-walled elastic tube which is mounted between two rigid tubes and enclosed in a pressure chamber. For sufficiently large chamber pressures, an initially circular cylindrical tube tends to buckle non-axisymmetrically. Once it has reached this configuration, the system readily develops large-amplitude self-excited oscillations when the imposed flow rate exceeds a certain threshold. In an attempt to predict the critical flow rate beyond which these oscillations develop, we showed in Whittaker *et al.* (7; 8) that in a certain parameter regime, the leading-order oscillatory components of the pressure and axial velocity are uniform in each cross-section. This leads to a spatially one-dimensional model, not dissimilar to the models used in the studies referred to above.

Within all spatially one-dimensional models, conservation of mass and Poiseuille's law (or another friction model) provide two equations involving the three unknowns u, p_{int} and A. A third equation — commonly known as a 'tube law' — is required to capture the wall mechanics in order to link the cross-sectional area A with the internal pressure p_{int} and thus close the system.

The simplest tube laws are entirely local, in that the cross-sectional area A of the tube at a given axial position is assumed to be determined entirely by the properties of the tube (often taken to be axially uniform) and the transmural pressure (equal to the internal pressure p_{int} minus the external pressure p_{ext}) at that axial position. Such a relationship is usually expressed as

$$p_{\text{int}} - p_{\text{ext}} = P(A) \tag{1.1}$$

for some function P. The form of $P(A)$ typically shows three distinct regions. At sufficiently high transmural pressures, the tube cross-section is almost circular, and changes in area arise primarily from axisymmetric stretching. As the transmural pressure is reduced and becomes negative, tubes tend to buckle and assume a squashed quasi-elliptical shape. In this mode, changes in cross-sectional area are achieved by bending rather than stretching, and the tube is more compliant than in its axisymmetric state. Finally at more negative transmural pressures, opposite sites of the tube come into contact, and the compliance decreases again. These effects give rise to the characteristic shape of $P(A)$, as shown in Fig. 2.

A number of simple power law and polynomial models for $P(A)$ have been proposed, based

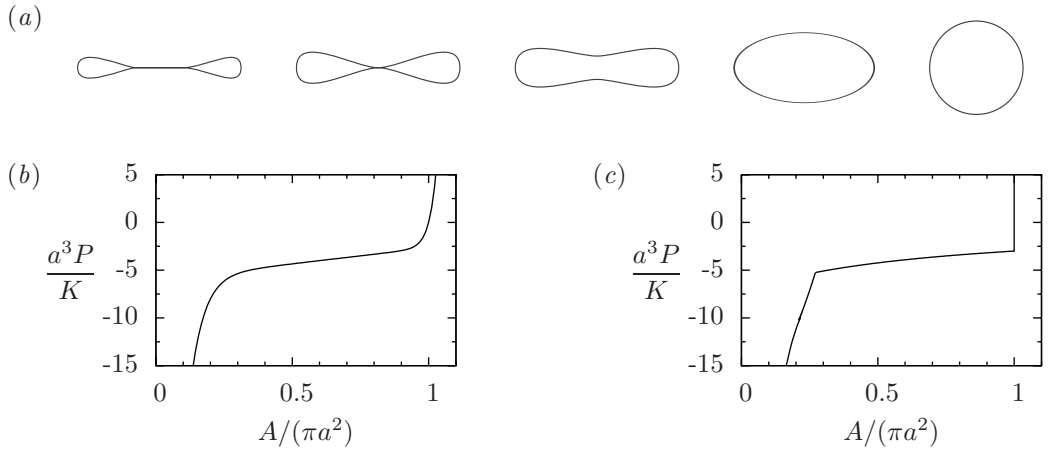

Fig. 2: *(a) Sketches of typical cross-sectional shapes of an initially circular elastic-walled tube under different transmural pressures, from most negative on the left to positive on the right. (b) A sketch of a typical experimental measurement of the pressure–area relationship $P(A)$ for a long tube, after Kececioglu* et al. *(9). (c) The theoretical result of Flaherty* et al. *(10) for an initially circular inextensible elastic ring with circumference $2\pi a$. K is the bending stiffness of the ring, as defined in (2.1b).*

on fitting to experimental or numerical data, see, for example, Shapiro (11), Kececioglu *et al.* (9), and Elad *et al.* (5). On the theoretical side, Tadjbakhsh and Odeh (12) and Flaherty *et al.* (10) calculated the deformations of an inextensible elastic ring under a uniform pressure loading. The resulting pressure–area relationship is shown in Fig. 2(c). The sharp corners arise through a buckling bifurcation from the circular state ($A = \pi a^2$), and the onset of opposite wall contact ($A \approx 0.27\pi a^2$).

However, these simple tube laws — with the pressure just being a function of the local area — fail to take into account any axial forces that may be present between neighbouring cross-sections as a result of the tube having axial variation in its cross-sectional shape. The addition of extra terms to account for axial stretching and bending was first considered theoretically by McClurken *et al.* (13) and also by Reyn (14).

McClurken *et al.* (13) assumed that the effects of axial tension (P_{T}) and axial bending (P_{B}) contribute additively to $P(A)$, so that

$$p_{\mathrm{int}} - p_{\mathrm{ext}} = P(A) + P_{\mathrm{T}} + P_{\mathrm{B}}\,. \tag{1.2}$$

To derive the form of P_{T}, they modelled the cross-section of a collapsed tube as a pair of parallel lines joined at each end by two semi-circles. The effects of axial tension on the two straight surfaces was then calculated and related to an equivalent pressure change. The result was an expression

$$P_{\mathrm{T}} = \frac{kT}{(\overline{A} - A)^{1/2}} \frac{\partial^2 A}{\partial z^2}\,, \tag{1.3}$$

where T is the axial tension, $\overline{A}$ is the area of the undeformed cross-section, z is the

axial coordinate, and k is a constant. (A similar expression was derived for P_{B} involving $\partial^4 A/\partial z^4$.)

Reyn (14) considered inflated tubes, whose axisymmetric shape allows the effect of axial tension to be calculated using membrane theory. For small amplitude deformations, an additive effect is found, again with $P_T \propto T\partial^2 A/\partial z^2$. He assumed that this form for P_T could still describe non-axisymmetric buckled tubes.

Neither of these approaches are particularly satisfactory, as they are based on the deformed tube adopting specific idealised geometries. Heil and Pedley (15) and Heil (16) also questioned the simple addition of a term of the form $T\partial^2 A/\partial z^2$, on the grounds that in a fully three-dimensional situation with a non-axisymmetric buckled tube, the sign of the term would not be obvious. They argued that in a cross-section of a buckled tube that is more collapsed then its neighbouring sections, the tension effects would act in the same direction as the (negative) transmural pressure near the (expanded) major axis, but in the opposite direction near the (contracted) minor axis. The formal analysis presented in this paper shows that the sign of the $T\partial^2 A/\partial z^2$ term is, in fact, correct. The existence of an azimuthal hoop stress leads to additional normal forces on the wall, which resolves the apparent discrepancy in the sign.

In this paper, we formally derive a tube law from shell theory that is valid for small-amplitude long-wavelength deformations of a thin-walled elliptical tube, and incorporates the leading-order effects of azimuthal bending and axial curvature. An elliptical cross-section is chosen as a simple model for the most compliant configuration of a collapsible tube (see Fig. 2), in which the fluid–structure interaction is strongest and which bypasses the discontinuities evident in Fig. 2(c). We show that the TA_{zz} term is indeed appropriate in this regime. Our systematic approach also shows which terms must be neglected to arrive at the simple tube law, and thus provides a means of understanding the regime in which such a tube law will hold, together with estimates of the likely errors for a given set of parameter values. Within the region of validity, the tube law enables us to capture the predictions of shell theory in a remarkably simple form. It can be combined with predictions of the flow in oscillating elliptical tubes (7; 8) to derive a rational asymptotic prediction for the onset of self-excited oscillations.

The paper is organised as follows. In §2 we define the geometry of the tube and the shell-theory model for the elastic walls, before considering the expected magnitude and form of the static deformations induced by an applied transmural pressure. In §3 we choose an appropriate non-dimensionalisation for the problem and derive the equations and boundary conditions governing the leading-order problem. This problem is solved using a pseudo-spectral method in §4 in order to obtain a tube law. In §5 we use the theoretical tube law to derive solutions for two simple cases (uniform and linearly varying transmural pressure applied to a finite-length tube with rigid supports) and compare these with numerical simulations. We present our conclusions in §6.

2. Setup

We consider a long thin-walled tube of length L, wall thickness d, and an axially-uniform elliptical cross-section with circumference $2\pi a$. In its undeformed elliptical state, the tube is subject to an axial pre-stress of magnitude $F/(2\pi ad)$, where F represents the extensional

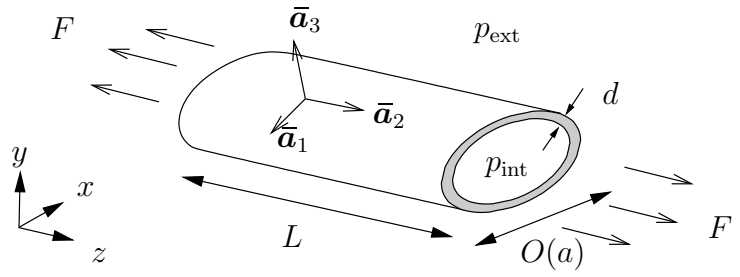

Fig. 3: *The setup of the tube in its undeformed elliptical configuration.*

force applied at the ends of the undeformed tube.[†] The tube is aligned with Cartesian coordinates (x, y, z), such that the tube axis lies along $x = y = 0$, and the major and minor axes are aligned with the x and y directions, respectively; see Fig. 3.

The tube wall is made of a linearly elastic material with incremental Young's modulus E and Poisson's ratio ν. We define the extensional stiffness D and bending stiffness K in the usual manner:

$$D = \frac{Ed}{1-\nu^2}\,, \qquad K = \frac{Ed^3}{12(1-\nu^2)}\,. \tag{2.1a,b}$$

Deformations to the undeformed state are then caused by a transmural pressure $p = p_{\text{int}} - p_{\text{ext}}$. The transmural pressure is assumed to have dimensional scale $\mathscr{P}$, and to vary only in the axial direction.[‡]

We define two dimensionless geometric parameters

$$\delta = \frac{d}{a}\,, \qquad \ell = \frac{L}{a}\,. \tag{2.2a,b}$$

We shall consider the regime in which $\ell \gg 1$ and $\delta \ll 1$, corresponding to a long thin-walled tube. Two further dimensionless parameters characterise the sizes of the applied pressure and axial tension relative to the bending stiffness of the tube, and we shall consider the regime in which

$$\frac{a^3\mathscr{P}}{K} \ll 1\,, \qquad \tilde{F} \equiv \frac{aF}{2\pi K\ell^2} = O(1)\,. \tag{2.3a,b}$$

We shall see in §2.3 below that these limits correspond to small-amplitude deformations in which the effects of the axial pre-stress and azimuthal bending both appear in the leading-order equilibrium equations.

We neglect any inertia associated with the tube wall. This corresponds to either considering the static case, or a regime where inertial effects are dominated by the inertia of the fluid filling the tube.

[†] With the pre-stress removed, the tube will no longer be elliptical or have uniform elastic properties. However, we adopt this configuration for simplicity, and do not consider the required form of the un-pre-stressed state.

[‡] This is consistent with the leading-order pressure field inside a fluid-filled tube in the long-wavelength limit, see e.g. Whittaker *et al.* (7).

2.1 *Coordinate system and tensor notation*

The mid-plane of the tube wall is parameterised by the Lagrangian coordinates (x^1, x^2), which, in the undeformed state, are taken to be measures of arc-length in the azimuthal and axial directions respectively. In the standard manner (see, e.g., 17; 18), the undeformed and deformed configurations of the tube are given respectively by the locations $\bar{\boldsymbol{r}}(x^1, x^2)$ and $\boldsymbol{r}(x^1, x^2)$ of the wall mid-plane for each (x^1, x^2). In the deformed state, we define the basis vectors and metric tensor

$$\boldsymbol{a}_\alpha = \boldsymbol{r}_{,\alpha} \equiv \frac{\partial \boldsymbol{r}}{\partial x^\alpha}\,, \qquad a_{\alpha\beta} = \boldsymbol{a}_\alpha \cdot \boldsymbol{a}_\beta\,, \tag{2.4a,b}$$

where Greek indices range over $(1, 2)$ and a subscript comma is used to denote partial derivatives. We also define the unit normal to the shell at each point

$$\boldsymbol{a}_3 = \frac{\boldsymbol{a}_1 \times \boldsymbol{a}_2}{|\boldsymbol{a}_1 \times \boldsymbol{a}_2|}\,, \tag{2.4c}$$

and the curvature tensor

$$b_{\alpha\beta} = \boldsymbol{a}_3 \cdot \boldsymbol{a}_{\alpha,\beta}\,. \tag{2.5}$$

Corresponding quantities $\bar{\boldsymbol{a}}_\alpha$, $\bar{\boldsymbol{a}}_3$, $\bar{a}_{\alpha\beta}$ and $\bar{b}_{\alpha\beta}$ are defined relative to the undeformed geometry.

2.2 *Shell theory and constitutive laws*

We use Kirchhoff–Love shell theory (19) to model the tube wall. This theory reduces the three-dimensional equations of elasticity to two dimensions, by making assumptions about the behaviour of the shell in the third (normal) direction. When combined with a constitutive law, the resulting equations relate the deformations of the shell's mid-plane to the external forces and moments acting on the shell's surfaces and boundary edges.

As shown in Fig. 4, the internal in-plane stress and stress moment resultants are represented by the tensors $N^{\alpha\beta}$ and $M^{\alpha\beta}$, while the normal stress resultant is Q^α. The externally applied tangential stress components, normal stress and stress moments are denoted f^α, f^3, and m^α respectively.

In covariant differential form and in the absence of shell inertia (see 17; 20, for example†), the Kirchhoff–Love shell equations are

$$N^{\alpha\beta} b_{\alpha\beta} + \nabla_\alpha Q^\alpha + f^3 = 0\,, \tag{2.6a}$$

$$\nabla_\beta N^{\beta\alpha} - b^\alpha_\gamma Q^\gamma + f^\alpha = 0\,, \tag{2.6b}$$

$$\nabla_\beta M^{\beta\alpha} - Q^\alpha + m^\alpha = 0\,. \tag{2.6c}$$

These equations represent the equilibrium of forces in the normal $\boldsymbol{a}_3$ direction and $\boldsymbol{a}_\alpha$ direction respectively, and moments about the two axes in the plane of the shell. The symbol

† Note that there are many different sign conventions and notations in use. In particular, Flügge (17) uses the opposite sign for $\kappa_{\alpha\beta}$, $M^{\alpha\beta}$, Q^α and m^α, while Søndergaard (20) uses $d^\beta_\alpha = -b^\beta_\alpha$. In Flügge (17), the equations are written in terms of the coordinates in the undeformed configuration, whereas here we use the coordinates of the deformed state.

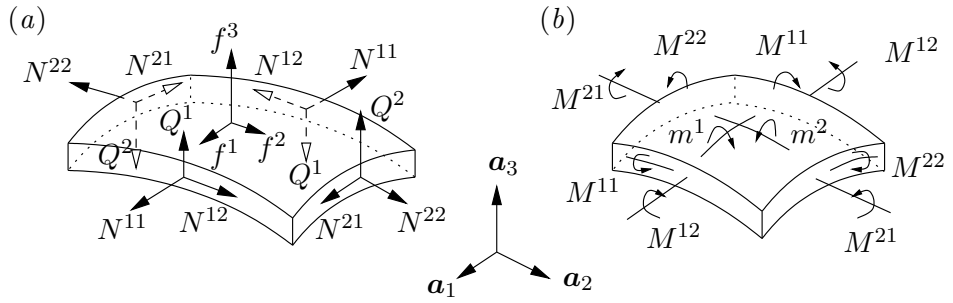

Fig. 4: *A shell element, depicting various components of the internal stress resultants and applied external forces. (a) The in-plane stress $N^{\alpha\beta}$, the normal shear stress Q^α and applied body force f^i. (b) The in-plane bending moment $M^{\alpha\beta}$ and the applied body moments m^α.*

∇_α represents the two-dimensional covariant derivative in the direction corresponding to the index α.

We now assume that the external forces arise solely from the transmural pressure, so that $f^\alpha = m^\alpha = 0$ and $f^3 = p$. Eliminating the normal stress resultant Q^α from (2.6), we then obtain

$$\nabla_\alpha \nabla_\beta M^{\alpha\beta} + N^{\alpha\beta} b_{\alpha\beta} = -p\,, \tag{2.7a}$$

$$\nabla_\beta N^{\beta 1} - b^1_\gamma \nabla_\beta M^{\beta\gamma} = 0\,, \tag{2.7b}$$

$$\nabla_\beta N^{\beta 2} - b^2_\gamma \nabla_\beta M^{\beta\gamma} = 0\,. \tag{2.7c}$$

The deformation of the wall material is characterised by in-plane strain and bending strain tensors

$$\gamma_{\alpha\beta} = \frac{1}{2}\Big(a_{\alpha\beta} - \overline{a}_{\alpha\beta}\Big)\,, \qquad \kappa_{\alpha\beta} = -b_{\alpha\beta} + \bar{b}_{\alpha\beta} + 2\bar{b}^\delta_\alpha \gamma_{\delta\beta}\,, \tag{2.8a,b}$$

where overbars denote the values of quantities in the undeformed configuration.

Linear constitutive laws relate the stress and stress moment resultants $N^{\alpha\beta}$ and $M^{\alpha\beta}$ to the strains $\gamma_{\alpha\beta}$ and $\kappa_{\alpha\beta}$ as follows (17, §9.4):†

$$\begin{aligned} N^{\alpha\beta} = {} & \delta^\alpha_2 \delta^\beta_2 \frac{F}{2\pi a} + D\left[(1-\nu)\gamma^{\alpha\beta} + \nu\gamma^\lambda_\lambda a^{\alpha\beta}\right] \\ & + K\left\{\frac{(1-\nu)}{2}\left[2a^{\beta\delta}b^{\alpha\gamma} + a^{\beta\gamma}b^{\alpha\gamma} + a^{\alpha\delta}b^{\beta\gamma} - b^\lambda_\lambda(a^{\alpha\delta}a^{\beta\gamma} + a^{\alpha\gamma}a^{\beta\delta})\right]\right. \\ & \qquad \left. + \nu\left[a^{\alpha\beta}b^{\gamma\delta} + a^{\gamma\delta}b^{\alpha\beta} - a^{\alpha\beta}a^{\gamma\delta}b^\lambda_\lambda\right]\right\}\kappa_{\gamma\delta}\,, \end{aligned} \tag{2.9a}$$

$$\begin{aligned} M^{\alpha\beta} = {} & K\left[-(1-\nu)(b^\alpha_\gamma\gamma^{\gamma\beta} - b^\lambda_\lambda\gamma^{\alpha\beta}) - \nu(b^{\alpha\beta} - b^\lambda_\lambda a^{\alpha\beta})\gamma^\mu_\mu\right. \\ & \left. + \tfrac{1}{2}(1-\nu)(\kappa^{\alpha\beta} + \kappa^{\beta\alpha}) + \nu a^{\alpha\beta}\kappa^\lambda_\lambda\right]\,. \end{aligned} \tag{2.9b}$$

† Some signs in (2.9) differ from those in Flügge (17). This is due to our opposing sign conventions on $\kappa_{\alpha\beta}$ and $M^{\alpha\beta}$, and later because of a sign error on the $(\kappa_{\alpha\beta} + \kappa_{\beta\alpha})$ term in Flügge's expression for $M^{\alpha\beta}$.

These constitutive laws arise from inserting the plane-stress form of Hooke's law into the definitions of $N^{\alpha\beta}$ and $M^{\alpha\beta}$, rewriting the resulting equations in terms of $\gamma_{\alpha\beta}$ and $\kappa_{\alpha\beta}$, and neglecting some higher-order terms in δ.

2.3 *Deformation magnitude and constraints*

To make analytic progress, we need to know which terms make up the dominant balances in (2.7). To achieve this, we must determine the relative sizes of the various terms in the constitutive laws (2.9), and this in turn requires the determination of the sizes of the deformations induced by a transmural pressure of typical size $\mathscr{P}$.

The detailed calculations can be found in Appendix A. We find that for small-amplitude deformations in the regime $\delta \ll 1$, $\ell \gg 1$, the possible dominant physical mechanisms that balance the transmural pressure are azimuthal bending and the action of the axial tension through axial curvature.

When $\tilde{F} = O(1)$, the estimates derived in Appendix A show that these two effects both contribute at leading order. In this case, the size of the deformations is found to be $O(\epsilon a)$ in the radial $\bar{\boldsymbol{a}}_3$ and azimuthal $\bar{\boldsymbol{a}}_1$ directions, and $O(\epsilon a/\ell, \epsilon a \delta^2 \ell)$ in the axial $\bar{\boldsymbol{a}}_2$ direction, where

$$\epsilon = \frac{a^3 \mathscr{P}}{K}\,. \tag{2.10}$$

To achieve small amplitude deformations, we must therefore ensure that $\mathscr{P}$ is chosen such that $\epsilon \ll 1$.

Since the shell is thin, it prefers to bend rather than stretch or shear. We show in Appendix A that the deformations have the property that there is little azimuthal stretching or in-plane shearing, so that

$$\gamma_{11} \lesssim \epsilon \max\{\delta^2, \ell^{-2}\}\,, \tag{2.11a}$$

$$\nabla_1 \gamma_{12} \lesssim \frac{\epsilon}{a\ell} \max\{\delta^2, \ell^{-2}\}\,. \tag{2.11b}$$

Both γ_{11} and $\nabla_1\gamma_{12}$ must then be smaller than the simple order-of-magnitude estimates given in Table A would suggest. They therefore result in restrictions on the form the deformations can take. The restrictions (2.11) provide useful relationships between some of the deformation components (see §3.3 below).

2.4 *Elliptical coordinates and deformation notation*

Since we are considering an elliptical tube, it is convenient to introduce a pair of dimensionless Lagrangian surface coordinates $\tau \in [0, 2\pi)$ and $z \in [0, 1]$ to replace the dimensional coordinates (x^1, x^2). The dimensionless coordinates are defined so that the Cartesian position vector of a general point on the mid-plane of the tube wall in the undeformed state is given by

$$\bar{\boldsymbol{r}} = a \begin{pmatrix} c\cosh\sigma_0 \cos\tau \\ c\sinh\sigma_0 \sin\tau \\ \ell z \end{pmatrix}\,, \tag{2.12}$$

where $\sigma_0 > 0$ defines the eccentricity of the cross-section, and $c = c(\sigma_0)$ is a normalisation factor chosen to set the circumference $\bar{C}$ of the undeformed configuration to be $2\pi a$ (see below).

The dimensionless surface coordinates are related to x^α by

$$\mathrm{d}x^1 = a\,h(\tau)\,\mathrm{d}\tau\,, \qquad \mathrm{d}x^2 = a\,\ell\,\mathrm{d}z\,, \tag{2.13a,b}$$

where

$$h(\tau) = c\Big(\sinh^2\sigma_0 + \sin^2\tau\Big)^{1/2} = c\Big(\tfrac{1}{2}\cosh 2\sigma_0 - \tfrac{1}{2}\cos 2\tau\Big)^{1/2}\,. \tag{2.14}$$

In the undeformed configuration, the circumference is

$$\overline{C} = a\int_0^{2\pi} h(\tau)\,\mathrm{d}\tau = 2\pi a\,\frac{2c\,\mathrm{Ee}(\operatorname{sech}\sigma_0)}{\pi\operatorname{sech}\sigma_0}\,, \tag{2.15}$$

where Ee is the complete elliptic integral of the second kind. To obtain $\overline{C} = 2\pi a$, we take

$$c = \frac{\pi\operatorname{sech}\sigma_0}{2\,\mathrm{Ee}(\operatorname{sech}\sigma_0)}\,. \tag{2.16}$$

The cross-sectional area is then given by

$$\overline{A} = \pi a^2\,\frac{c^2\sinh 2\sigma_0}{2} = \pi a^2\,\frac{\pi^2\tanh\sigma_0}{4[\mathrm{Ee}(\operatorname{sech}\sigma_0)]^2}\,. \tag{2.17}$$

Unit vectors in the normal and azimuthal directions to the undeformed surface are given respectively by

$$\hat{\boldsymbol{t}} \equiv \bar{\boldsymbol{a}}_1 = \frac{c}{h}\begin{pmatrix} -\cosh\sigma_0\sin\tau \\ \sinh\sigma_0\cos\tau \\ 0 \end{pmatrix}\,, \qquad \hat{\boldsymbol{z}} \equiv \bar{\boldsymbol{a}}_2 = \begin{pmatrix} 0 \\ 0 \\ 1 \end{pmatrix}\,, \tag{2.18a,b}$$

$$\hat{\boldsymbol{n}} \equiv \bar{\boldsymbol{a}}_3 = \frac{c}{h}\begin{pmatrix} \sinh\sigma_0\cos\tau \\ \cosh\sigma_0\sin\tau \\ 0 \end{pmatrix}\,. \tag{2.18c}$$

We represent the normal, tangential, and axial displacements of the wall with the dimensionless functions $(\xi, \eta, \zeta, \zeta_a)$, by writing the location $\boldsymbol{r}$ of the surface element initially at $\bar{\boldsymbol{r}}(\tau, z)$ as

$$\boldsymbol{r} = \bar{\boldsymbol{r}}(\tau,z) + \frac{\epsilon a}{h(\tau)}\Big(\xi(\tau,z)\hat{\boldsymbol{n}} + \eta(\tau,z)\hat{\boldsymbol{t}}\Big) + \epsilon a\ell\left(\frac{1}{\ell^2}\,\zeta(\tau,z) + \delta^2\,\zeta_a(z)\right)\hat{\boldsymbol{z}}\,. \tag{2.19}$$

where

$$\int_0^{2\pi}\zeta(\tau,z)\,h(\tau)\,\mathrm{d}\tau = 0\,. \tag{2.20}$$

The various pre-factors in (2.19) have been chosen to yield the correct scales for the deformation components when $\xi, \eta, \zeta, \zeta_a = O(1)$. Two different functions are required to capture the axial displacements because they are induced by two different physical mechanisms that lead to different scales and functional forms. (See the determination of the scales ϵ'_τ and ϵ'_z in Appendix A.) The factor $h(\tau)$ is introduced for mathematical convenience in the calculations that follow.

The tube law we are about to derive describes the geometry of the tube in terms of its cross-sectional area. The change in area must therefore be related to the deformation functions $\xi, \eta, \zeta, \zeta_a$. We find that

$$A - \overline{A} = \oint (\boldsymbol{r} - \bar{\boldsymbol{r}}) \cdot \hat{\boldsymbol{n}} \, \mathrm{d}x^1 + O(\epsilon^2) = \epsilon a^2 \int_0^{2\pi} \xi \, \mathrm{d}\tau + O(\epsilon^2) \,. \tag{2.21}$$

3. Leading-order asymptotic limit

3.1 *Scaling and non-dimensionalisation*

We now non-dimensionalise the stresses, strains, and curvatures in the problem, taking care to choose appropriate scales. We introduce non-dimensional variables for the key components, while just estimating the magnitudes of the higher-order components that do not enter our model.

The transmural pressure $p = p_{\mathrm{int}} - p_{\mathrm{ext}}$ is non-dimensionalised on the scale $\mathscr{P} = \epsilon K / a^3$, appropriate by construction. We write

$$p = \frac{\epsilon K}{a^3} \tilde{P} \,. \tag{3.1}$$

We also recall the definition of the scaled axial force $\tilde{F}$ in (2.3b).

In the undeformed state, there is only one non-zero component of the curvature tensor $\bar{b}^\beta_\alpha$. This is the azimuthal curvature, which has size $O(1/a)$. We therefore write

$$\bar{b}^\beta_\alpha = \frac{1}{a} \begin{bmatrix} \overline{B}(\tau) & 0 \\ 0 & 0 \end{bmatrix} . \tag{3.2}$$

The normal displacements of $O(\epsilon a)$ may change the azimuthal curvature by $O(\epsilon/a)$. The assumed slow axial variation over the length scale L means the other curvature components are smaller by factors of ℓ on purely geometric grounds. We therefore write

$$b^\beta_\alpha = \bar{b}^\beta_\alpha + \frac{\epsilon}{a h(\tau)} \begin{bmatrix} \beta(\tau, z) & O(\ell^{-1}) \\ O(\ell^{-1}) & \dfrac{1}{\ell^2} \mathbb{B}_{\mathrm{n}}(\tau, z) \end{bmatrix} , \tag{3.3}$$

(The factor of $h(\tau)$ is found to be mathematically convenient for the analysis that follows, and the subscript 'n' in $\mathbb{B}_{\mathrm{n}}$ is to indicate that the curvature arises from the axial variation of normal displacements.) We retain the axial curvature even though it is formally of smaller magnitude, since that component will later be multiplied by the large axial tension to produce an $O(1)$ effect.

Using scaling estimates based on the sizes of the deformations and the additional relations (2.11) we see that the in-plane strain $\gamma_{\alpha\beta}$ can be written as

$$\gamma_{\alpha\beta} = \epsilon \begin{bmatrix} O(\delta^2, \ell^{-2}) & \dfrac{1}{\ell}\Big(s(z) + O(\delta^2, \ell^{-2})\Big) \\ \dfrac{1}{\ell}\Big(s(z) + O(\delta^2, \ell^{-2})\Big) & \dfrac{1}{\ell^2}\dfrac{\partial \zeta}{\partial z} + \delta^2 \dfrac{\mathrm{d}\zeta_a}{\mathrm{d}z} + \dots \end{bmatrix} , \tag{3.4a}$$

where we have introduced $s(z)$ as the leading-order component of the shear strain. This is independent of τ by virtue of (2.11b).

From the expressions (2.8b) and (3.3), the bending strain $\kappa_{\alpha\beta}$ can be written as

$$\kappa_{\alpha\beta} = \frac{\epsilon}{a}\begin{bmatrix} -\dfrac{1}{h}\beta + O(\delta^2, \ell^{-2}) & \dfrac{1}{\ell}O(1) \\ \dfrac{1}{\ell}O(1) & -\dfrac{1}{\ell^2 h}\mathbb{B}_{\mathrm{n}} \end{bmatrix}, \tag{3.4b}$$

The in-plane stress $N^{\alpha\beta}$ has a component due to the axial pre-stress, to which the perturbations forced by the applied pressure forcing are added. From (2.9a) and (3.4a), we have

$$N^{\alpha\beta} = \frac{K}{a^2}\begin{bmatrix} 0 & 0 \\ 0 & \ell^2\tilde{F} \end{bmatrix} + \frac{\epsilon K}{a^2}\begin{bmatrix} \tilde{N}(\tau, z) & \ell\tilde{S}(z) + \dots \\ \ell\tilde{S}(z) + \dots & \tilde{\Sigma}(\tau, z) \end{bmatrix}, \tag{3.5}$$

where $\tilde{F}$ is the scaled axial pre-stress defined in (2.3b), $\tilde{N}(\tau, z)$ is the dimensionless hoop stress (to be determined),

$$\tilde{S}(z) = \frac{12(1-\nu)\, s(z)}{\delta^2\ell^2} \tag{3.6}$$

is the leading-order dimensionless shear stress, and

$$\tilde{\Sigma}(\tau, z) = \nu\tilde{N} + 12(1-\nu^2)\left(\frac{1}{\delta^2\ell^2}\frac{\partial\zeta}{\partial z} + \frac{\mathrm{d}\zeta_a}{\mathrm{d}z}\right) + \dots \tag{3.7}$$

is the dimensionless axial stress. (Note that the constraint (A11) means that $\tilde{S} \le O(1)$ regardless of the value of $\delta^2\ell^2$.)

The bending moment $M^{\alpha\beta}$ is given in terms of the strains and curvatures in (2.9b). From (3.4a), the strains $\gamma_{\alpha\beta}$ that appear in $M^{\alpha\beta}$ are small enough not to contribute at leading order. From the curvature terms (3.4b) that do contribute, we obtain

$$M^{\alpha\beta} = -\frac{\epsilon K}{a}\begin{bmatrix} \dfrac{1}{h}\beta + O(\delta^2, \ell^{-2}) & O(\ell^{-1}) \\ O(\ell^{-1}) & O(\ell^{-2}) \end{bmatrix}. \tag{3.8}$$

To obtain the non-dimensional form of the governing equations, we must also evaluate the two covariant derivatives that appear in (2.7). At leading order these are given by

$$\nabla_1 = \frac{1}{ah}\frac{\partial}{\partial\tau} + O(\ell^{-1}), \qquad \nabla_2 = \frac{1}{a\ell}\frac{\partial}{\partial z} + O(\ell^{-2}). \tag{3.9a,b}$$

We also need to include one of the higher-order terms when computing the derivative of $N^{\alpha\beta}$ in (2.7) owing to the large factor multiplying the pre-stress $\tilde{F}$. The full expression is

$$\nabla_\alpha N^{\alpha\beta} = \frac{\partial N^{\alpha\beta}}{\partial x^\alpha} + \Gamma^\beta_{\mu\nu}N^{\mu\nu}, \tag{3.10}$$

where $\Gamma^\beta_{\mu\nu} \equiv a^{\alpha\beta}\boldsymbol{a}_\alpha \cdot \boldsymbol{a}_{\mu,\nu}$ is the Christoffel symbol. The relevant additional term is the one containing $\Gamma^1_{22} = O(\epsilon\ell^{-2})$. We express Γ^1_{22} as

$$\Gamma^1_{22} = \frac{\epsilon}{a\ell^2 h}\mathbb{B}_{\mathrm{t}} + \dots. \tag{3.11}$$

where the new scaled quantity $\mathbb{B}_{\mathrm{t}} = O(1)$ is related to component of the surface curvature arising from axial variations in the tangential displacements (hence the subscript 't').

3.2 *Leading-order equilibrium equations*

We now substitute the expressions (3.1)–(3.11) above into the governing equations (2.7). Retaining only the leading order terms in ϵ, δ and ℓ^{-1}, we obtain

$$\overline{B}\tilde{N} + \frac{\tilde{F}\,\mathbb{B}_{\rm n}}{h} - \frac{1}{h}\frac{\partial}{\partial\tau}\left[\frac{1}{h}\frac{\partial}{\partial\tau}\left(\frac{\beta}{h}\right)\right] + \tilde{P} = 0\,, \tag{3.12a}$$

$$\frac{\partial\tilde{N}}{\partial\tau} + h\frac{\mathrm{d}\tilde{S}}{\mathrm{d}z} + \tilde{F}\,\mathbb{B}_{\rm t} + \overline{B}\frac{\partial}{\partial\tau}\left(\frac{\beta}{h}\right) = 0\,, \tag{3.12b}$$

$$\nu\frac{\mathrm{d}}{\mathrm{d}z}\left(\frac{1}{2\pi}\int_0^{2\pi}\tilde{N}h\,\mathrm{d}\tau\right) + 12(1-\nu^2)\frac{\mathrm{d}^2\zeta_a}{\mathrm{d}z^2} = 0\,. \tag{3.12c}$$

The third equation (3.12c), which arises from the axial force balance, has been averaged over the azimuthal coordinate. The azimuthal variation in the axial force balance involves higher-order quantities, and decouples at leading order.

3.3 *Curvature components in terms of displacements*

We now evaluate the various dimensionless curvature and shear components $(\overline{B}, \beta, \mathbb{B}_{\rm n}, \mathbb{B}_{\rm t}, \tilde{S})$ introduced above in terms of the deformation functions $(\xi, \eta, \zeta, \zeta_a)$. The detailed calculations can be found in Appendix B, where we obtain

$$\overline{B} = -\frac{c^2\sinh 2\sigma_0}{2h^3}\,, \tag{3.13a}$$

$$\beta = \frac{-2}{c^2\sinh 2\sigma_0}\frac{\partial}{\partial\tau}\left(1 + \frac{\partial^2}{\partial\tau^2}\right)\eta\,, \tag{3.13b}$$

$$\mathbb{B}_{\rm n} = \frac{\partial^2\xi}{\partial z^2}\,, \tag{3.13c}$$

$$\mathbb{B}_{\rm t} = \frac{\partial^2\eta}{\partial z^2}\,, \tag{3.13d}$$

$$\tilde{S} = \frac{12(1-\nu)}{\delta^2\ell^2}\frac{\mathrm{d}}{\mathrm{d}z}\left(\frac{1}{2\pi}\int_0^{2\pi}\eta\,\mathrm{d}\tau\right)\,. \tag{3.13e}$$

It is unnecessary to evaluate $\tilde{N}$ as it will be eliminated from the governing equations in §3.4 below.

We also show in Appendix B that the following relationships hold at leading order:

$$\xi\sinh 2\sigma_0 + \frac{2h^2}{c^2}\frac{\partial\eta}{\partial\tau} - \eta\sin 2\tau = 0\,, \tag{3.14a}$$

$$\frac{\partial\eta}{\partial z} + \frac{\partial\zeta}{\partial\tau} = \frac{h(\tau)}{2\pi}\frac{\mathrm{d}}{\mathrm{d}z}\left(\int_0^{2\pi}\eta\,\mathrm{d}\tau\right)\,. \tag{3.14b}$$

Equations (3.14) arise from the estimates (2.11a) and (2.11b) on the size of the in-plane strains, which imply that there is negligible azimuthal stretching and that the in-plane shear is uniform in each cross-section. They allow the determination of ξ and ζ in terms of η. (The constant of integration in the latter case being set by (2.20).) Equation (3.12c) can be used to recover ζ_a, subject to suitable boundary conditions at $z = 0, 1$.

3.4 *Reduction to a single equation for η*

We now eliminate the hoop stress $\tilde{N}$ between (3.12b) and (3.12a), and substitute for $\overline{B}$, $\mathbb{B}_{\rm n}$, $\mathbb{B}_{\rm t}$ and $\tilde{S}$ from (3.13). We obtain

$$\mathscr{L}(\beta) = \tilde{P}C_P h + h\frac{\mathrm{d}^2}{\mathrm{d}z^2}\mathscr{I}(\eta) + \tilde{F}\left[\left(C_n + C_{n'}\frac{\partial}{\partial\tau}\right)\frac{\partial^2\xi}{\partial z^2} + \frac{\partial^2\eta}{\partial z^2}\right], \tag{3.15}$$

where the linear operators $\mathscr{L}$ and $\mathscr{I}$ are given by

$$\mathscr{L}(\beta) \equiv \frac{2}{c^2\sinh 2\sigma_0}\left(\frac{\partial^3}{\partial\tau^3} + L_2\frac{\partial^2}{\partial\tau^2} + L_1\frac{\partial}{\partial\tau} + L_0\right)\beta\,, \tag{3.16a}$$

$$\mathscr{I}(\eta) \equiv \frac{12(1-\nu)}{\delta^2\ell^2}\frac{1}{2\pi}\int_0^{2\pi}\eta\,\mathrm{d}\tau\,, \tag{3.16b}$$

and the coefficients L_i and are

$$L_2 = -\frac{3\sin 2\tau}{\cosh 2\sigma_0 - \cos 2\tau}\,, \tag{3.17a}$$

$$L_1 = -\frac{(2\cos^2 2\tau + 8\cosh 2\sigma_0\cos 2\tau - 9 - \cosh^2 2\sigma_0)}{(\cosh 2\sigma_0 - \cos 2\tau)^2}\,, \tag{3.17b}$$

$$L_0 = \frac{3\sin 2\tau\,(\cosh^2 2\sigma_0 - 5 + 4\cosh 2\sigma_0\cos 2\tau)}{(\cosh 2\sigma_0 - \cos 2\tau)^3}\,. \tag{3.17c}$$

The coefficients on the right-hand side of (3.15) are

$$C_P = \frac{3\sin 2\tau}{\sinh 2\sigma_0}\,,\quad C_n = \frac{2\sin 2\tau}{\sinh 2\sigma_0}\,,\quad C_{n'} = \frac{(\cosh 2\sigma_0 - \cos 2\tau)}{\sinh 2\sigma_0}\,. \tag{3.18a–c}$$

We eliminate ξ and β from (3.15) using (3.14a) and (3.13b) to obtain

$$\mathscr{L}\big(\mathscr{K}(\eta)\big) - h\frac{\partial^2}{\partial z^2}\mathscr{I}(\eta) - \tilde{F}\frac{\partial^2}{\partial z^2}\mathscr{J}(\eta) = \tilde{P}(z)C_p h\,, \tag{3.19}$$

where

$$\mathscr{K}(\eta) \equiv \frac{-2}{c^2\sinh 2\sigma_0}\frac{\partial}{\partial\tau}\left(1 + \frac{\partial^2}{\partial\tau^2}\right)\eta = \beta\,, \tag{3.20a}$$

$$\begin{aligned}\mathscr{J}(\eta) \equiv &-\frac{\big(\cosh 2\sigma_0 - \cos 2\tau\big)^2}{\sinh^2 2\sigma_0}\frac{\partial^2\eta}{\partial\tau^2} - \frac{3\big(\cosh 2\sigma_0 - \cos 2\tau\big)\sin 2\tau}{\sinh^2 2\sigma_0}\frac{\partial\eta}{\partial\tau}\\ &+ \frac{2\sinh^2 2\sigma_0 + 3\sin^2 2\tau - \big(\cosh 2\sigma_0 - \cos 2\tau\big)^2}{\sinh^2 2\sigma_0}\eta\,.\end{aligned} \tag{3.20b}$$

Equation (3.19) is a partial integro-differential equation for $\eta(\tau, z)$, forced by the transmural pressure $\tilde{P}$. The equation is sixth order in τ and second order in z, and it is to be solved for $\tau \in (0, 2\pi)$, $z \in (0, 1)$.

3.5 *Boundary conditions*

The boundary conditions at $\tau = 0, 2\pi$ arise from the requirement that η be 2π-periodic in τ. Similar periodicity conditions apply to ξ, β and ζ. We also require boundary conditions at $z = 0$ and $z = 1$, which arise from specifying conditions at the ends of the elastic tube. Physically, we expect to be able to either hold the tube in a fixed position (pinned or clamped) or allow it to be free to move (force-free). However, we do not have enough degrees of freedom to apply the full set of boundary conditions that can usually be applied in shell theory, and the conditions we do apply must be consistent with the relations (3.14) that arose from the approximations we made.

Since we have reduced the system to an equation in the azimuthal displacement η, we first consider the boundary conditions on η. Since (3.19) is second order in z we require one condition on η at $z = 0$ and one condition at $z = 1$. The simplest condition to impose is to pin $\eta = 0$ at both ends.

The conditions imposed on ξ, ζ and ζ_a must now be consistent with the equations through which they are recovered from η. Equation (3.14a) is used to recover the normal displacement ξ without further integration, and implies we must take $\xi = 0$ at $z = 0, 1$ too. However, we are unable to simultaneously impose $\zeta = \zeta_a = 0$ or $\partial\xi/\partial z = 0$, as we would do for a fully clamped condition on a shell, as we now explain.

The axial displacement component ζ is recovered from η using (3.14b), with the constant of integration set by (2.20). We will not, in general, obtain $\zeta = 0$ at $z = 0, 1$. The displacements ζ_a are recovered using (3.12c). This equation is second order in z, but only one-dimensional, being averaged over τ. We can therefore only apply either an integrated condition or a condition at a single point in τ on the full axial displacements at each end of the tube. The simplest option is to specify $\zeta_a = 0$ at $z = 0, 1$.

Taken together, these conditions correspond to a fixed tube cross-section at each end, but with displacements in the axial direction allowed, subject to their azimuthal mean being zero.

Applying additional boundary conditions on ζ, ζ_a or $\partial\xi/\partial z$ in a full shell problem would result in violations of our modelling assumptions at least in the neighbourhood of the ends. We expect to see boundary effects near $z = 0$ and $z = 1$, which may or may not disrupt the solution in the bulk of the shell.

For the development of the tube law, we assume the restricted boundary conditions described above. In §5, we shall compare the results with numerical simulations in which the full shell equations are subjected to a variety of different boundary conditions. This will reveal the regimes under which the solutions subject to the restricted boundary conditions described above are a good approximation.

4. Solution via Fourier decomposition

4.1 *Uniqueness and symmetries of the solutions*

In Appendix C we show that the solution $\eta(\tau, z)$ to the system (2.7) with a given $\tilde{P}$ and homogeneous boundary conditions is unique, and must be odd and π-periodic in τ. From (3.13b) and (3.14a), we see that the corresponding solutions for β and ξ are even and π-periodic in τ. Since η is odd in τ, we have $\mathscr{I}(\eta) \equiv 0$, and the governing equation (2.7) becomes a PDE.

Owing to the symmetries present in the solutions, we are able to restrict our domain from

$0 < \tau < 2\pi$ to $0 < \tau < \pi/2$. The boundary conditions on η are then

$$\eta = \frac{\partial^2 \eta}{\partial \tau^2} = \frac{\partial^4 \eta}{\partial \tau^4} = 0 \quad \text{on} \quad \tau = 0, \pi/2\,, \tag{4.1a–c}$$

$$\eta = 0 \quad \text{on} \quad z = 0, 1\,. \tag{4.1d}$$

It is easy to see that the symmetric continuation of a solution of (3.19) on $0 < \tau < \pi/2$ satisfying these conditions to the full domain $0 < \tau < 2\pi$ will satisfy (3.19) and the full set of boundary conditions.

4.2 *Fourier expansions*

Owing to the symmetry of the solution, it is convenient to express η as a Fourier series

$$\eta = \sum_{n=1}^{\infty} e_n(z) \sin(2n\tau)\,. \tag{4.2a}$$

Substituting this expansion into (3.13b) and (3.14a) we obtain the corresponding series

$$\xi = \sum_{n=1}^{\infty} \frac{e_n(z)}{\sinh 2\sigma_0} \Big\{ \big(n + \tfrac{1}{2}\big) \cos\big(2[n-1]\tau\big) - 2n \cosh 2\sigma_0 \cos(2n\tau) + \big(n - \tfrac{1}{2}\big) \cos\big(2[n+1]\tau\big) \Big\}\,, \tag{4.2b}$$

$$\beta = \sum_{n=1}^{\infty} \frac{4n(4n^2-1)}{c^2 \sinh 2\sigma_0}\, e_n(z)\, \cos(2n\tau)\,. \tag{4.2c}$$

Using (2.21) and (2.17), the fractional area change $\epsilon\alpha$ is given by

$$\alpha(z) \equiv \frac{A(z) - \overline{A}}{\epsilon \overline{A}} = \frac{6\, e_1(z)}{c^2\, \sinh^2 2\sigma_0}\,. \tag{4.3}$$

Therefore only the first Fourier mode of the solution contributes to changes in the cross-sectional area at this order of approximation.

4.3 *Decomposition of* η

Using the Fourier representations (4.2) and recalling that $\mathscr{I}(\eta) = 0$, we may re-express (3.19) as

$$\mathscr{L}(\mathscr{K}(\eta)) = \tilde{P}(z)\, C_p(\tau)\, h(\tau) + \tilde{F} \sum_{m=1}^{\infty} C_{T\,m}(\tau)\, e_m''(z)\,, \tag{4.4}$$

where

$$C_{T\,m}(\tau) = \frac{1}{\sinh^2 2\sigma_0} \Big\{ \Big[3\sin^2 2\tau + 2\sinh^2 2\sigma_0 + (4m^2-1)(\cosh 2\sigma_0 - \cos 2\tau)^2 \Big] \sin(2m\tau) - 6m\, (\cosh 2\sigma_0 - \cos 2\tau)\, \cos(2m\tau)\, \sin 2\tau \Big\}\,. \tag{4.5}$$

The first term on the right-hand side of (4.4) represents forcing of the azimuthal bending in a cross-section directly from the applied transmural pressure. The sum in the second term represents axial tension effects arising from interactions with neighbouring cross-sections with different cross-sectional shapes. Each term in the sum comes from a different Fourier mode of the cross-sectional deformation. We now decompose η into parts due to these different effects.

We define the functions $\eta^{(P)}(\tau)$ and $\eta_m^{(T)}(\tau)$ to satisfy

$$\mathscr{L}(\mathscr{K}(\eta^{(P)})) = C_p h\,, \qquad \mathscr{L}(\mathscr{K}(\eta_m^{(T)})) = C_{T\,m}(\tau)\,, \tag{4.6a,b}$$

together with the homogeneous boundary conditions (4.1) that apply to the full solution η. Since $\mathscr{L}$ and $\mathscr{K}$ are linear, and the solution η is known to be unique, we then have that

$$\eta(\tau, z) = \tilde{P}(z)\,\eta^{(P)}(\tau) + \tilde{F}\sum_{m=1}^{\infty} \eta_m^{(T)}(\tau)\,b_m''(z)\,. \tag{4.7}$$

We define Fourier series for $\eta^{(P)}$ and $\eta_m^{(T)}$ in the natural way as

$$\eta^{(P)}(\tau) = \sum_{n=1}^{\infty} E_n^{(P)} \sin(2n\tau)\,, \qquad \eta_m^{(T)}(\tau) = \sum_{n=1}^{\infty} E_{mn}^{(T)} \sin(2n\tau)\,, \tag{4.8a,b}$$

and equating coefficients in (4.7), we obtain

$$e_n(z) = \tilde{P}(z)\,E_n^{(P)} + \tilde{F}\sum_{m=1}^{\infty} E_{mn}^{(T)}\,e_m''(z)\,. \tag{4.9}$$

This gives a set of evolution equations for $e_n(z)$ in terms of the coefficients $E_n^{(P)}$ and $E_{mn}^{(T)}$. The problem is now reduced to evaluating these coefficients.

4.4 *Evaluation of $E_m^{(P)}$ and $E_{mn}^{(T)}$*

To compute $E_m^{(P)}$ and $E_{mn}^{(T)}$, one approach is to use a full spectral method, evaluating the Fourier expansion of each side of (4.6). However, the decompositions are not convenient to perform, owing to the square root in $h(\tau)$ (see (2.14)) and the multiple products of trigonometric functions of τ in the coefficients of $\mathscr{L}$ (see (3.16) and (3.17)).

Instead we solve (4.6) directly for $\eta^{(P)}(\tau)$ and $\eta_m^{(T)}(\tau)$, and then compute the Fourier coefficients $E_n^{(P)}$ and $E_{mn}^{(T)}$ from the numerical solutions. We find that a very good approximation can be obtained by truncating after the first ($m = 1$) term in (4.9), and this method recovers $E_1^{(P)}$ and $E_{11}^{(T)}$ with less effort.

For a given σ_0, equation (4.6a) is solved numerically using a shooting technique. The system is split into a set of six coupled first-order equations, and a fourth-order Runge–Kutta scheme is used to integrate from $\tau = 0$ to $\tau = \pi/2$. At $\tau = 0$, we fix $\partial^n \eta^{(P)}/\partial\tau^n = 0$ for $n = 0, 2, 4$ and adjust the remaining derivatives until we obtain $\partial^n \eta^{(P)}/\partial\tau^n = 0$ at $\tau = \pi/2$ for $n = 0, 2, 4$.

Once the solution for $\eta^{(P)}$ is found, corresponding solutions for $\beta^{(P)}$ and $\xi^{(P)}$ can be

recovered using (3.13b) and (3.14a). We also compute the first few Fourier coefficients in the series (4.8a) from the numerical solution using

$$E_n^{(P)} = \frac{1}{\pi}\int_0^{\pi} \eta^{(P)}(\tau)\,\sin(2n\tau)\,\mathrm{d}\tau\,. \tag{4.10}$$

The same procedure is used for $\eta_1^{(T)}$ and $\eta_2^{(T)}$, which are forced in (4.6b) by

$$C_{T1} = \frac{1}{\sinh^2 2\sigma_0}\Big[6\,(\cosh 2\sigma_0 - \cos 2\tau)^2 - \sinh^2 2\sigma_0\Big]\sin 2\tau\,, \tag{4.11a}$$

$$C_{T2} = \frac{2}{\sinh^2 2\sigma_0}\Big[-42\cos^2 2\tau\cosh 2\sigma_0 + 6\cosh 2\sigma_0 + 24\cos^3 2\tau - 5\cos 2\tau + 17\cos 2\tau\cosh^2 2\sigma_0\Big]\sin 2\tau\,. \tag{4.11b}$$

The numerical solutions for the normal displacement ξ, azimuthal displacement η, and curvature perturbation β with $\sigma_0 = 0.6$ are shown in Fig. 5. We also plot the first and second partial sums from the Fourier expansions (4.8). We see in Fig. 5 that, while there is a clear contribution to β from higher frequency ($n > 1$) modes, the contribution to the displacement fields (ξ, η) is negligible.

The numerically computed leading Fourier coefficients $E_i^{(P)}$, $E_{1i}^{(T)}$ and $E_{2i}^{(T)}$ for $i = 1, 2$ are plotted as functions of the ellipticity parameter σ_0 in Fig. 6. For $E_i^{(P)}$ and $E_{1i}^{(T)}$ it can be seen that the amplitude of the second Fourier mode remains very much less than that of the fundamental mode even for fairly small σ_0 (strongly elliptical tubes). The amplitude of the second mode of the displacement field is reduced even more, owing to the smoothing effect of the operator in (3.13b). The amplitude ratio is less in the case of $E_{2i}^{(T)}$, but this is less important since these terms will be seen to relate higher-order effects which already have small amplitudes themselves.

4.5 *The tube law*

We now consider an approximation in which the deformations that result from a cross-sectionally uniform transmural pressure $\tilde{P}(z)$ and axial pre-stress $\tilde{F}$ are modelled by just the first Fourier mode in (4.2) and (4.8). This means that we truncate the coefficients relation (4.9) after $m = 1$. In doing so, we obtain a closed-form equation for $e_1(z)$:

$$e_1(z) = E_1^{(P)}\,\tilde{P}(z) + \tilde{F}\,E_{11}^{(T)}\,\frac{\partial^2 e_1}{\partial z^2}\,. \tag{4.12}$$

This approximation is justified by the relative sizes of the coefficients $E_i^{(P)}$ and $E_{ij}^{(T)}$. As $E_2^{(P)} \ll E_1^{(P)}$ and $E_{i2}^{(T)} \ll E_{i1}^{(T)}$ (Fig. 6), we expect the amplitude of $e_2(z)$ to be much smaller than that of $e_1(z)$. Hence its neglected contribution in (4.12) will be negligible. Similar arguments apply to $e_3(z)$ and higher-order modes.

The expression (4.3) gives the relative area change $\epsilon\alpha \equiv (A - \overline{A})/\overline{A}$ in terms of the Fourier coefficient $e_1(z)$. Using this result, (4.12) can be rewritten as

$$\tilde{P} = k_0\,\alpha - k_2\tilde{F}\,\frac{\partial^2\alpha}{\partial z^2}\,, \tag{4.13}$$

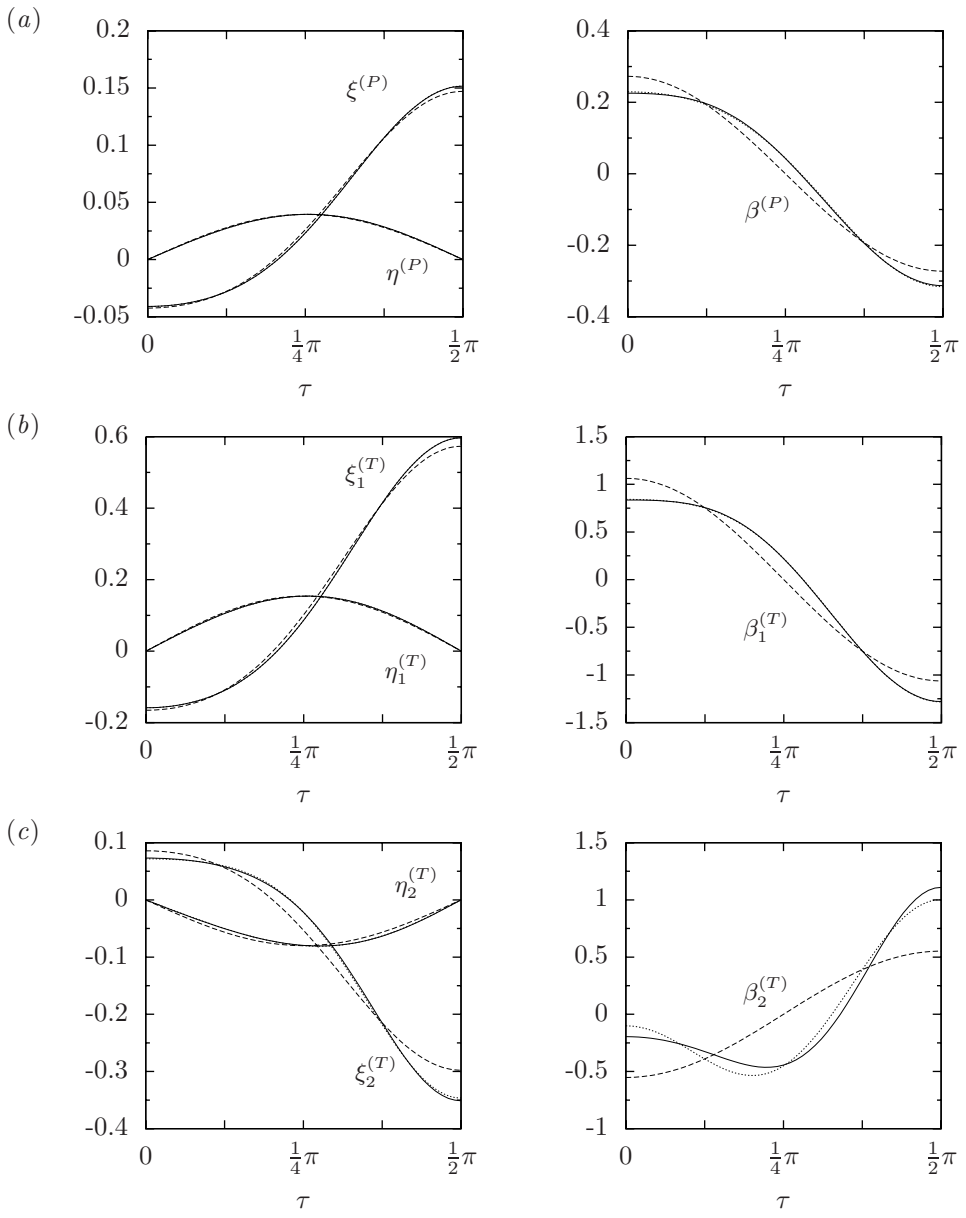

Fig. 5: *Solutions to (4.6) for $\eta^{(P)}$ and $\eta_m^{(T)}$ with $\sigma_0 = 0.6$, also showing the corresponding ξ and β fields, as functions of the azimuthal coordinate τ. Continuous lines show the full numerical solutions to (4.6). The dashed lines are the components of each solution corresponding to the $n = 1$ Fourier modes in (4.2). The dotted lines (many almost indistinguishable from the corresponding solid lines) include the contribution from the $n = 2$ modes as well.*

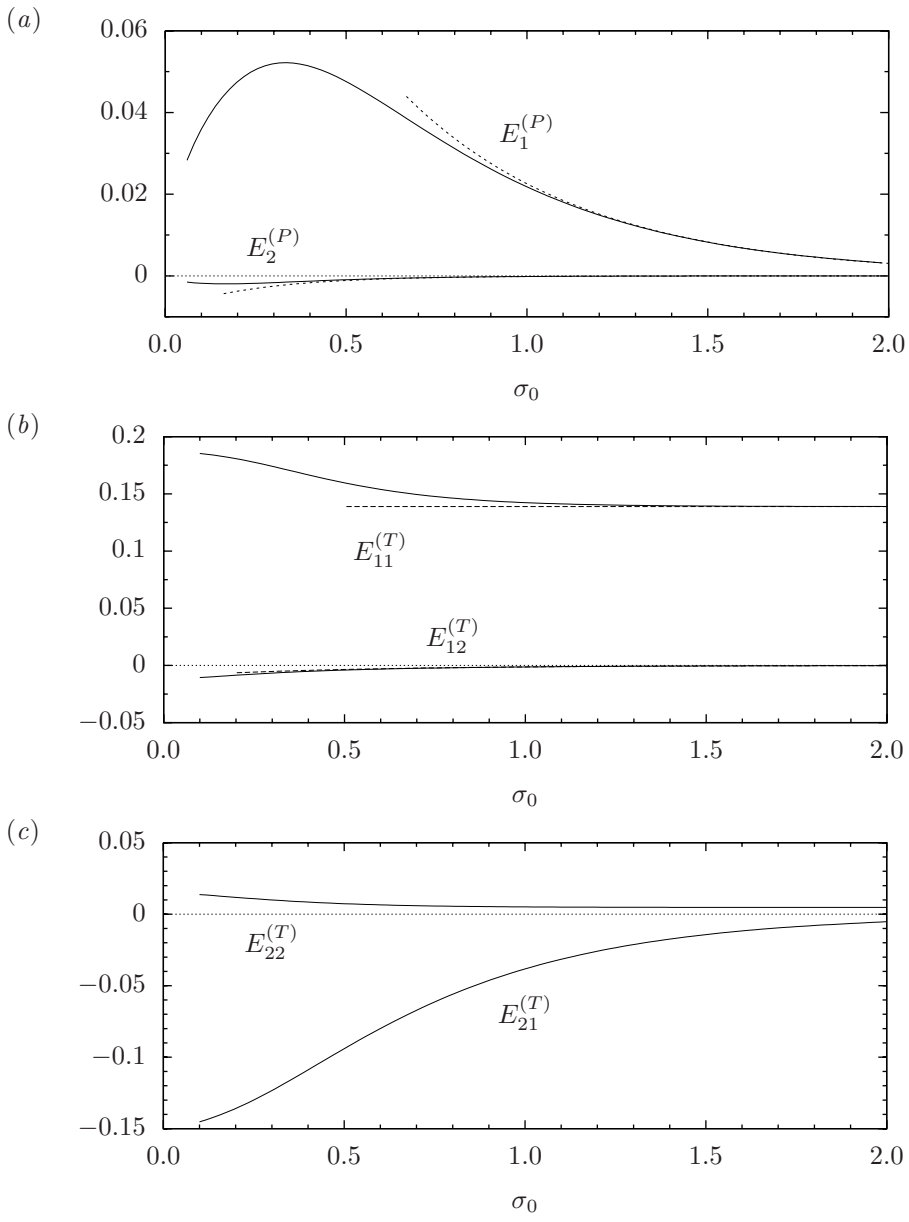

Fig. 6: *The leading Fourier coefficients in the expansions (4.8) of* $\eta^{(P)}$ *and* $\eta_m^{(T)}$ *as functions of the ellipticity parameter* σ_0*. The solid lines are computed from the numerical solutions to (4.6) using (4.10). The dashed lines are the leading order asymptotic solutions to (4.6) as* $\sigma_0 \to \infty$ *(i.e. as the tube cross-section becomes circular). They are obtained analytically and have the form the form* $E\mathrm{e}^{-n\sigma_0}$ *for some constant* E *and integer* n*.*

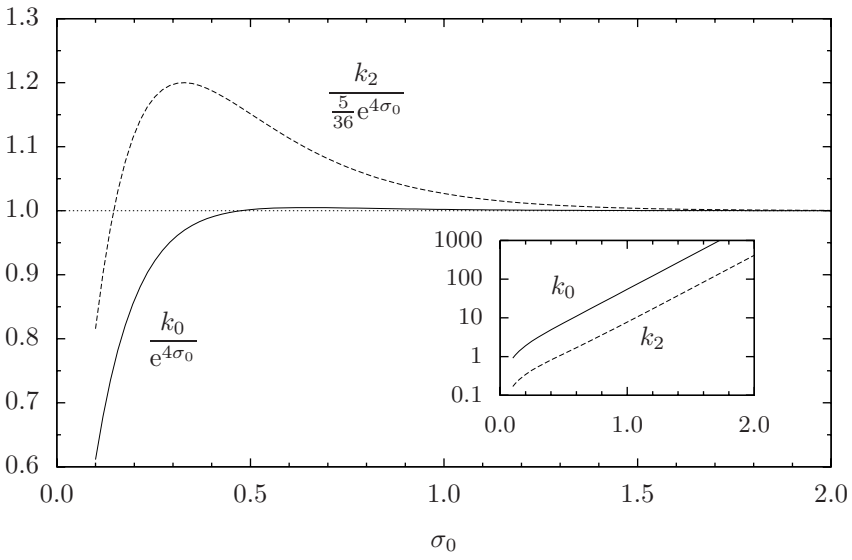

Fig. 7: *The dimensionless coefficients k_0 (solid) and k_2 (dashed) from (4.13) as functions of the ellipticity parameter σ_0. In the main graph the curves are scaled by the asymptotic expressions $k_0 \sim e^{4\sigma_0}$ and $k_2 \sim \frac{5}{36}e^{4\sigma_0}$ as $\sigma_0 \to \infty$. The inset shows a logarithmic plot.*

where the coefficients k_i are given by

$$k_0 = \frac{c^2 \sinh^2(2\sigma_0)}{6E_1^{(P)}}, \qquad k_2 = \frac{c^2 \sinh^2(2\sigma_0)\, E_{11}^{(T)}}{6E_1^{(P)}}. \tag{4.14a,b}$$

Equation (4.13) is a tube law that links the relative change α in cross-sectional area to the transmural pressure $\tilde{P}$. The two coefficients k_i are plotted as functions of σ_0 in Fig. 7. Observe that even for σ_0 as low as 0.2 (corresponding to an elliptical cross-section whose semi-axes have a ratio of just over $5:1$) the coefficients differ by less than 20% from their asymptotic forms as $\sigma_0 \to \infty$.

5. Comparison with numerical simulations

5.1 *Setup*

To assess the validity of the tube law, we now present comparisons with numerical computations. The computations were performed using the open-source `oomph-lib` library (21) and its built-in discretisation of the thin-shell equations. We consider an elliptical tubes with ellipticity parameter $\sigma_0 = 0.6$ (corresponding to a semi-axis ratio of $1.86:1$). Calculations were performed with both a uniform ($\tilde{P} = -1$) and linearly varying ($\tilde{P} = -2z$) transmural pressure, resembling typical loads arising in fluid-loaded tubes. At the tube ends, the following three sets of boundary conditions were used:

1. *Clamped* — The position and gradient of the surface are fixed, so that $\xi = \eta = \zeta = \zeta_a = 0$ and $\partial\xi/\partial z = 0$.

2. *Pinned* — The position of the points at the tube end is fixed ($\xi = \eta = \zeta = \zeta_a = 0$) but the slope is free, subject to zero torque.
3. *Sliding* — Only the normal and tangential positions are fixed ($\xi = \eta = 0$). The axial displacements ζ, ζ_a and the slope $\partial\xi/\partial z$ are free, but subject to zero torque and an axial stress equal to $\mathscr{F}/(2\pi)$.

The clamped condition is physically the most relevant if we are considering a flexible tube attached to rigid supports (as would be the case in a Starling resistor setup). However, the sliding condition corresponds most closely to the conditions used in the modelling (see §3.5). As we shall see below, the choice of boundary condition can have quite a significant effect on the solutions obtained.

5.2 *Tube-law predictions for simple pressure profiles*

The solutions of (4.13) with $\tilde{P} = -1$ and $\tilde{P} = -2z$, subject to $\alpha(0) = \alpha(1) = 0$, are given by

$$\alpha(z) = -\frac{1}{k_0}\left(1 - \frac{\cosh\lambda(z-\frac{1}{2})}{\cosh(\frac{1}{2}\lambda)}\right) \qquad [\tilde{P} = -1]\,, \tag{5.1a}$$

$$\alpha(z) = -\frac{2}{k_0}\left(z - \frac{\sinh\lambda z}{\sinh\lambda}\right) \qquad [\tilde{P} = -2z]\,, \tag{5.1b}$$

where

$$\lambda^2 = \frac{k_0}{k_2\tilde{F}}\,. \tag{5.2}$$

With $\sigma_0 = 0.6$, the coefficients are given by $k_0(0.6) = 11.075$ and $k_2(0.6) = 1.7044$.

5.3 *Numerical Results*

We compared the tube-law predictions (5.1) with results from numerical simulations for tubes with ellipticity parameter $\sigma_0 = 0.6$ and pressure scale $\epsilon = 0.2$, and a range of different values of aspect ratios ℓ, wall thicknesses δ, and axial tensions $\tilde{F}$. All three boundary conditions were tested, and a selection of results are shown in Figs. 8–12.

As expected from the fact that the tube-law theory was developed for the $\ell \gg 1$ and $\delta \ll 1$ asymptotic regime, we found we needed to take $\ell \gtrsim 10$ and $\delta \lesssim 0.1$ to obtain a good description of the numerical results. More surprisingly, we also found that the clamped and pinned boundary conditions required a further constraint $\delta^2\ell^3 \gtrsim 10$, whereas this was not required for the sliding condition. In all of our results, there was little noticeable difference between the pinned and clamped boundary conditions, indicating that the bending boundary layer has negligible effect on the solutions for $\ell \gg 1$. The effects of the boundary conditions are discussed in greater detail in §5.4 below.

When comparing the results, we first checked the key assumption of the model that the deformation of each cross-section is dominated by a single mode shape. To this end, we note that if the displacements ξ and η are given by just the $n = 1$ Fourier mode in the expansions (4.2), then the ratios ξ/α and η/α are independent of the amplitude e_1 and hence of the axial position z. We therefore evaluate ξ/α and η/α from the numerical results and plot these quantities as functions of the azimuthal coordinate τ for several different values of z.

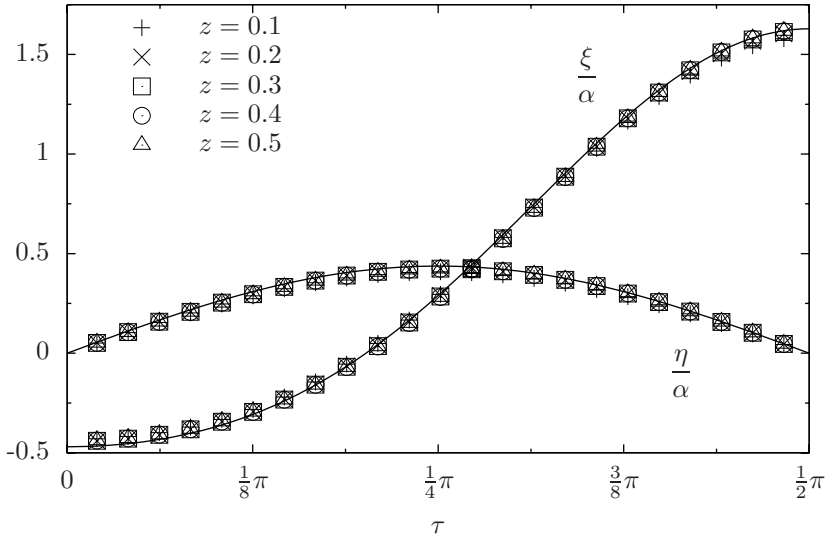

Fig. 8: *Scaled cross-sectional deformations $\xi(\tau, z)/\alpha(z)$ and $\eta(\tau, z)/\alpha(z)$ at a number of axial positions z for a uniform pressure $\tilde{P} = -1$. The other parameters are $\sigma_0 = 0.6$, $\epsilon = 0.2$, $\ell = 20$, $\delta = 0.05$, and $\tilde{F} = 1$. Points represent the numerical results for which we used we used clamped boundary conditions at the tube ends. The lines are the first ($n = 1$) Fourier modes in the expansions (4.2).*

A typical plot is shown in Fig. 8. The predicted independence of z is indeed observed, and there is excellent agreement between the numerical results and the predicted modes.

Secondly, we compared the axial variation of the cross-sectional area $A(z)$ — the quantity that the tube law aims to predict. Typical solutions showing good agreement for all boundary conditions are presented in Fig. 9 (uniform pressure) and Fig. 10 (linearly varying pressure). Solutions showing a marked discrepancy between the sliding boundary condition and the clamped and pinned conditions are shown in Fig. 11. In the following section, we shall discuss the origin of this discrepancy and the region of parameter space in which it occurs.

5.4 *Effect of the tube-end boundary conditions*

For $\ell \gg 1$, our numerical results with the clamped and pinned boundary conditions are almost the same, suggesting that the effects of the bending boundary layer are negligible in this regime.

However, for certain values of δ and ℓ (such as in Fig. 11), the results obtained with the sliding boundary condition are significantly different from those obtained with the clamped or pinned boundary conditions. In these cases, the tube-law predictions appear to describe the numerical results with the sliding boundary condition, but not those with the clamped or pinned conditions.

We believe that the differences arise due to the clamped and pinned boundary conditions

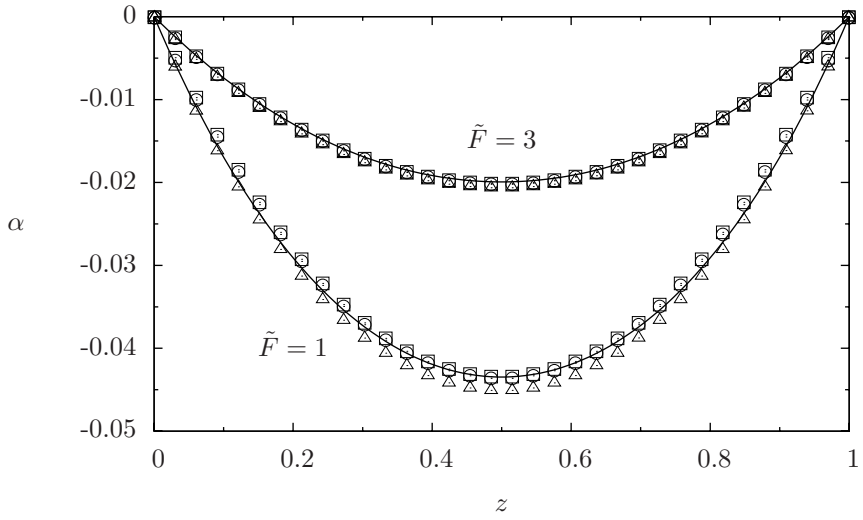

Fig. 9: *The change in cross-sectional area as a function of axial position z for a uniform pressure $\tilde{P} = -1$, with $\sigma_0 = 0.6$, $\epsilon = 0.2$, $\ell = 20$, and $\delta = 0.05$. The continuous lines are the theoretical result (5.1a), while the points are from numerical simulations: squares for the clamped boundary condition, circles for pinned and triangles for sliding.*

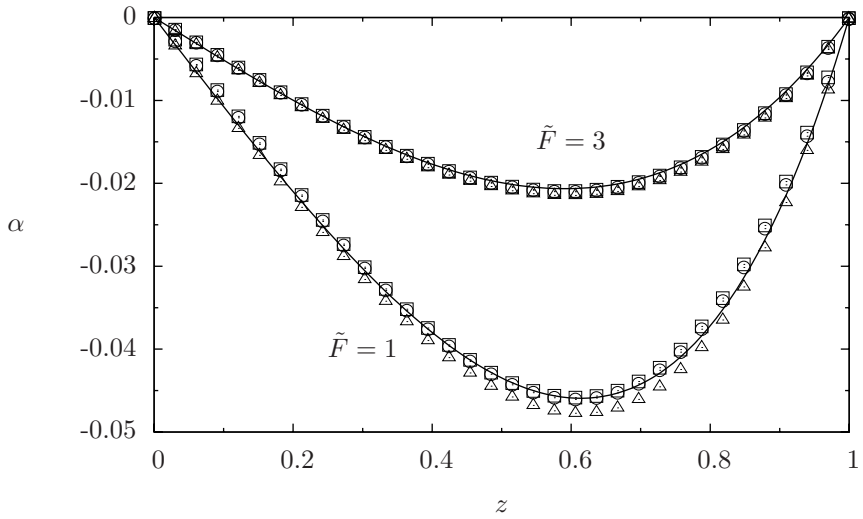

Fig. 10: *The change in cross-sectional area as a function of axial position z for a linearly varying pressure $\tilde{P} = -2z$, with $\sigma_0 = 0.6$, $\epsilon = 0.2$, $\ell = 20$, and $\delta = 0.05$. The continuous lines are the theoretical result (5.1b), while the points are from numerical simulations: squares for the clamped boundary condition, circles for pinned and triangles for sliding.*

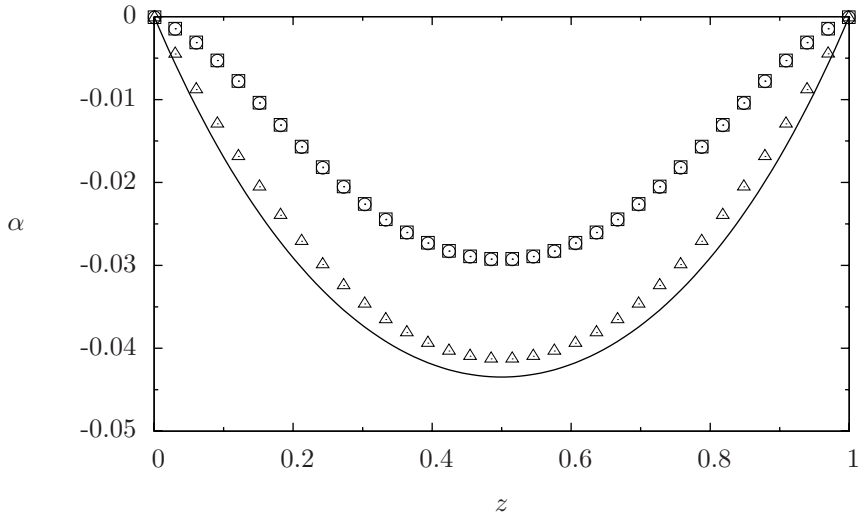

Fig. 11: *The change in cross-sectional area as a function of axial position z for a uniform pressure $\tilde{P} = -1$ with $\sigma_0 = 0.6$, $\epsilon = 0.2$, $\ell = 20$, $\delta = 0.01$, , and $\tilde{F} = 1$. The continuous lines are the theoretical result (5.1a), while the points are from numerical simulations: squares for the clamped boundary condition, circles for pinned and triangles for sliding. The solution with the sliding boundary conditions is well-described by the theory, but the other two solutions are not.*

causing a violation of the 'negligible shear' assumption (2.11b) used in the model. With the sliding condition, the tube is free to slide axially at the ends, and we obtain a non-zero ζ. This situation is depicted in Fig. 12(a). The axial displacements are able to arrange themselves so that shearing is minimal. With clamped or pinned boundary conditions, the tube cannot move axially at the ends, so some shearing is inevitable. The question now is whether the forces associated with that shearing are large enough to disrupt the leading-order balances.

We estimate the magnitude of the forces by considering the typical (dimensional) force F_e required to eliminate the axial displacements that occur with the sliding boundary condition. We then compare the (dimensional) moment M_e generated by these axial forces (which alternate in sign around the perimeter) with the (dimensional) moment M_p generated by the applied transmural pressure acting over the rest of the tube.

We estimate F_e as the shear force required to give axial displacements of $O(\epsilon a/\ell)$ varying on the $O(a)$ lengthscale around the circumference. We therefore obtain $F_e \sim \epsilon D a/\ell$. The moment is then the force times a typical length around the perimeter, so $M_e \sim F_e a$. Using $D \sim K/(\delta^2 a^2)$ from (2.1), we arrive at

$$M_e \sim \frac{\epsilon K}{\delta^2 \ell} \tag{5.3}$$

The force due to the pressure has size $F_p \sim \mathscr{P} a L \sim \epsilon K \ell / a$, and is applied at lengths of

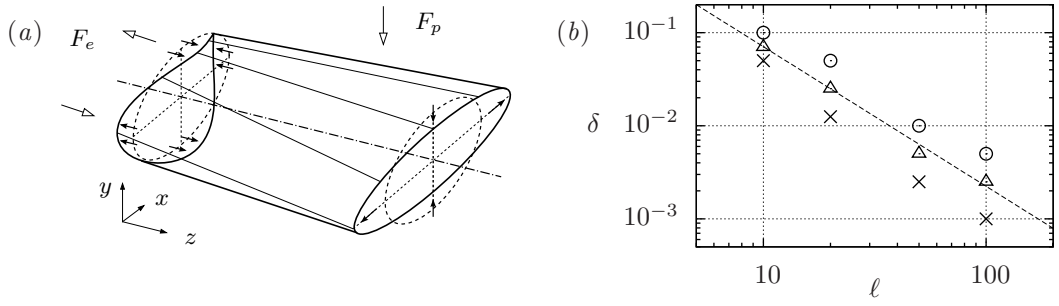

Fig. 12: *(a) An exaggerated sketch depicting the axial displacements that occur at the tube end (in order to avoid shearing) when using the 'sliding' boundary conditions. Also shown are the force F_p from the transmural pressure, and the axial forces F_e required at the boundary to achieve $\zeta = 0$ with pinned or clamped conditions. (b) The regions of ℓ–δ space affected by the use of non-sliding boundary conditions. We computed the relative error χ in $A - \bar{A}$ at $z = 1/2$ between the model and the numerical results. Circles indicate negligible effect ($|\chi| < 0.02$, as in Fig. 9), crosses a significant effect ($|\chi| > 0.1$, as in Fig. 11), and triangles borderline cases ($0.02 < |\chi| < 0.1$). The dashed line is $\delta^2\ell^3 = 5$, which is consistent with the theoretical arguments presented in §5.4.*

$O(L)$ away from the tube end. Hence the moment is given by

$$M_p \sim \epsilon K \ell^2 \tag{5.4}$$

For the effect of a non-sliding boundary condition to be negligible, we must have $M_e \ll M_p$, i.e.

$$\delta^2\ell^3 \gg 1\,. \tag{5.5}$$

We tested this constraint by performing simulations at various points in δ–ℓ space, and examining them visually to see if the effects of the different boundary conditions are evident. The results are shown in Fig. 12(b). These results support (5.5); the tube-law approximation works well for clamped or pinned boundary conditions provided $\delta^2\ell^3 \gtrsim 10$.

6. Discussion and Conclusions

By taking a formal asymptotic limit of a shell-theory model, and then considering the fundamental mode of cross-sectional deformations, we have derived a tube-law (4.13) governing small-amplitude long-wavelength deformations of an initially elliptical thin-walled elastic tube. In dimensional form, the tube law can be written as

$$p_{\text{int}} - p_{\text{ext}} = \frac{k_0 K}{a^3}\left(\frac{A - \overline{A}}{\overline{A}}\right) - \frac{k_2 F}{2\pi}\frac{\partial^2}{\partial z^{*2}}\left(\frac{A - \overline{A}}{\overline{A}}\right), \tag{6.1}$$

where $p_{\text{int}} - p_{\text{ext}}$ is the transmural pressure, K is the bending stiffness of the tube wall, $2\pi a$ is the circumference of the undeformed tube, F is the axial stretching force, A is the cross-sectional area, $\overline{A}$ is the area in the undeformed state, and $z^* = a\ell z$ is the dimensional

axial coordinate. The dimensionless coefficients k_0 and k_2 are numerically determined, and depend on the ellipticity of the undeformed state (see Fig. 7). The tube law (6.1) has a form that has commonly been used in previous work, but our derivation allows the calculation of the coefficients and also provides further insight into when the law might break down and how it could be refined further.

For a tube of length L and wall thickness d, with deformations of typical amplitude ϵa, our modelling formally applies in the limit $\ell \equiv L/a \gg 1$, $\delta \equiv d/a \ll 1$, $\epsilon \equiv a^3\mathscr{P}/K \ll 1$. In part because the tube law is only second order in the axial coordinate z^*, and in part because of the shell's resistance to shearing, one needs to be careful when relating boundary conditions at the tube end to those to be applied to the tube law equation (6.1). With some boundary conditions in some regions of parameter space, the tube law is no longer a good model for the deformations. We find that for the common physical 'clamped' conditions in which the tube wall position and axial slope are fixed at the ends, the appropriate boundary conditions for (6.1) are $A = \overline{A}$ at each end, and that the predictions from the tube law are good provided provided $\delta^2\ell^3 \gg 1$. (Outside this limit, the boundary conditions prevent the neglect of shear forces, and the tube law is no longer an appropriate description of the resulting deformations; see §5.4.) In practice we find that $\ell \geq 10$, $\delta \leq 0.1$ and $\delta^2\ell^3 \geq 10$ are sufficient to give predictions of the tube shape with clamped boundary conditions with errors of less than 5% when compared with the numerical solution of the full shell equations.

One key approximation in deriving (6.1) is the assumption that the azimuthal deformation at each axial position is dominated by the same single mode shape. This is justified by the numerical results, which show (e.g. in Fig. 8) that deformations are indeed well-described by this mode at the small amplitudes considered here. It would be relatively straightforward to include additional deformation modes (i.e. truncate the representation (4.9) at $n = 2$ or higher), though this would result in a more complicated tube law: we would obtain a coupled set of equations relating the pressure to the cross-sectional area and the amplitudes of higher-order modes.

In terms of other extensions and improvements to the simple tube law (6.1), it would be straightforward to allow for an azimuthally non-uniform transmural pressure by writing it as a Fourier series

$$\tilde{P}(\tau, z) = \sum_{n=0}^{\infty} \tilde{P}_n(z)\cos(2n\tau)\,, \tag{6.2}$$

and including the first few terms. (The inclusion of additional deformation modes, as described above, may become necessary for higher azimuthal wavenumbers.) One could also easily add the effects of shell inertia in the linearised equations (3.12). Further calculations in §4 would be unnecessary, since the inertial terms enter in the same way as the axial tension terms, but with $\partial^2\eta/\partial z^2$ replaced by $\partial^2\eta/\partial t^2$, and $\tilde{F}$ replaced by a non-dimensional mass per unit area.

Finally, we consider how this work might be extended to be applied to other initial cross-sectional shapes and larger amplitude deformations. It is highly likely that deformations of other simple cross-sectional shapes will also be dominated by a single deformation mode. While that mode would have to be determined numerically, a similar analysis to that performed here should be possible; the only difference in the resulting tube law being in the coefficients k_0 and k_2. The inclusion of geometric nonlinearities to take account of larger amplitude deformations is expected to be more problematic. Nevertheless it may be

possible to use the nonlinear response of an inextensible ring (12) as the dominant mode, and compute the (now) amplitude-dependent response from axial tension effects.

Having derived a tube law systematically from shell theory, we are now in a position to evaluate the modes of oscillation of a fluid-filled tube, and hence derive asymptotic conditions for the onset of global instability in collapsible tube flows. Results will be reported elsewhere (22).

Acknowledgements

The authors would like to acknowledge the financial support of the Engineering and Physical Sciences Research Council to undertake the project of which this work is a part. RJW and SLW are supported by grant EP/D070910/2; and MH by grant EP/D670422/1. SLW is also is grateful to the EPSRC for funding in the form of an Advanced Research Fellowship.

References

1. M. Heil and O. E. Jensen, Flows in deformable tubes and channels: Theoretical models and biological applications. In P. W. Carpenter and T. J. Pedley, editors, *Flow Past Highly Compliant Boundaries and in Collapsible Tubes*, chap. 2, pages 15–49, Kluwer Academic, Dordrecht, ISBN 1-402-01161-x (2003).

2. J. B. Grotberg and O. E. Jensen, Biofluid mechanics in flexible tubes. *Annu. Rev. Fluid Mech.* **36** (2004) 121–147.

3. S. J. Sherwin, V. Franke, J. Peiro and K. Parker, One-dimensional modelling of vascular network in space-time variables. *J. Engr. Math.* **47** (2003) 217–250.

4. J.-M. Fullana and S. Zaleski, A branched one-dimensional model of vessel networks. *J. Fluid Mech.* **621** (2009) 183–204.

5. D. Elad, R. D. Kamm and A. H. Shapiro, Choking phenomena in a lung like model. *ASME J. Biomech. Engr* **109** (1987) 1–9.

6. K. Berkouk, P. W. Carpenter and A. D. Lucey, Pressure wave propagation in fluid-filled co-axial elastic tubes. part 1: Basic theory. *ASME J. Biomech. Engr* **125** (2003) 852–856.

7. R. J. Whittaker, S. L. Waters, O. E. Jensen, J. Boyle and M. Heil, The energetics of flow through a rapidly oscillating tube. Part I: General theory. *J. Fluid Mech.* Accepted for publication.

8. R. J. Whittaker, M. Heil, J. Boyle, O. E. Jensen and S. L. Waters, The energetics of flow through a rapidly oscillating tube. Part II: Application to an elliptical tube. *J. Fluid Mech.* Accepted for publication.

9. I. Kececioglu, M. E. McClurken, R. D. Kamm and A. H. Shapiro, Steady, supercritical flow in collapsible tubes. Part 1. Experimental observations. *J. Fluid Mech.* **109** (1981) 367–389.

10. J. E. Flaherty, J. Keller and S. I. Rubinow, Post-buckling behaviour of elastic tubes and rings with opposite sides in contact. *SIAM J. Appl. Math.* **23** (1972) 446–455.

11. A. H. Shapiro, Steady flow in collapsible tubes. *ASME J. Biomech. Engr* **99** (1977) 126–147.

12. I. Tadjbakhsh and F. Odeh, Equilibrium states of elastic rings. *J. Math. Anal. Appl.* **18** (1967) 59–74.

13. M. E. McClurken, I. Kececioglu, R. D. Kamm and A. H. Shapiro, Steady, supercritical flow in collapsible tubes. Part 2. Theoretical studies. *J. Fluid Mech.* **109** (1981) 391–415.

14. J. W. Reyn, Multiple solutions and flow limitation for steady flow through a collapsible tube held open at the ends. *J. Fluid Mech.* **174** (1987) 467–493.

15. M. Heil and T. J. Pedley, Large post-buckling deformations of cylindrical shells conveying viscous fluid. *J. Fluids Struct.* **10** (1996) 565–599.

16. M. Heil, Stokes flow in collapsible tubes: Computation and experiment. *J. Fluid Mech.* **353** (1997) 285–312.

17. W. Flügge, *Tensor Analysis and Continuum Mechanics*. Springer-Verlag (1972).

18. G. Wempner, *Mechanics of Solids with Applications to Thin Bodies*. McGraw–Hill, New York (1973), ISBN 0-070-69270-X.

19. A. E. H. Love, The small free vibrations and deformations of a thin elastic shell. *Phil. Trans. R. Soc. Lond. A* **179** (1888) 491–546.

20. N. Søndergaard, Moving frames applied to shell elasticity. *Journal of Physics A: Mathematical and Theoretical* **40** (2007) 5067–5081.

21. M. Heil and A. Hazel, Oomph-lib — an object-orientated multi-physics finite-element library. Open source software; available online at http://www.oomph-lib.org/ (2007).

22. R. J. Whittaker, M. Heil, O. E. Jensen and S. L. Waters, The onset of high-frequency self-excited oscillations in elastic-walled tubes. *Proc. R. Soc. A* Submitted.

APPENDIX A

Deformation size and constraints

In this appendix, we use scaling arguments and order-of-magnitude balances to estimate the typical size of the deformations that result from a transmural pressure of size $\mathscr{P}$ within a small amplitude thin-shell long-wavelength regime. We also show that the resulting deformations have the property that there is significantly less azimuthal stretching and azimuthal variation of the shear strain than would be suggested by a simple order-of-magnitude estimate based on scaling arguments alone.

A.1 *Stress scalings in terms of the deformations*

Tables A–C provide estimates for the normal and axial stress components appearing as terms in (2.7) that will arise in a deformed configuration in which material elements are displaced by an $O(a\epsilon)$ amount in the normal and azimuthal directions and amounts $O(a\epsilon'_\tau)$ and $O(a\epsilon'_z)$ axially. The two axial scales are necessary to distinguish between displacements that have azimuthal variation and those that do not, as the two have different magnitudes. We take the axial displcements of

	Mechanism	Strain	Dominant contribution to (2.7a)
Stretching	Azimuthal	$\gamma_{11} \sim \frac{\epsilon a}{a}$	$N^{11}b_{11} \sim \frac{D\gamma_{11}}{a} \sim \frac{\epsilon K}{a^3}\frac{1}{\delta^2}$
	Shear	$\gamma_{12} \sim \frac{\epsilon a}{L}, \frac{\epsilon'_\tau a}{a}$	$\nabla_1\nabla_2 M^{12} \sim \frac{K\gamma_{12}}{a^2 L} \sim \frac{\epsilon K}{a^3}\frac{1}{\ell^2}\left(1, \frac{\epsilon'_\tau \ell}{\epsilon}\right)$; $N^{12}b_{12} \sim D\gamma_{12}\kappa_{12} \sim \frac{\epsilon K}{a^3}\frac{\epsilon}{\delta^2\ell^2}\left(1, \frac{\epsilon'_\tau \ell}{\epsilon}\right)$
	Axial	$\gamma_{22} \sim \frac{\epsilon'_\tau a}{L}, \frac{\epsilon'_z a}{L}$	$N^{11}b_{11} \sim \nu\frac{D\gamma_{22}}{a} \sim \frac{\epsilon K}{a^3}\frac{1}{\delta^2}\left(\frac{\epsilon'_\tau}{\epsilon\ell}, \frac{\epsilon'_z}{\epsilon\ell}\right)$
Bending	Azimuthal	$\kappa_{11} \sim \frac{\epsilon a}{a^2}$	$\nabla_1\nabla_1 M^{11} \sim \frac{K\kappa_{11}}{a^2} \sim \frac{\epsilon K}{a^3}$
	Torsion	$\kappa_{12} \sim \frac{\epsilon a}{aL}$	$\nabla_1\nabla_2 M^{12} \sim \frac{K\kappa_{12}}{aL} \sim \frac{\epsilon K}{a^3}\frac{1}{\ell^2}$
	Axial	$\kappa_{22} \sim \frac{\epsilon a}{L^2}$	$\nabla_1\nabla_1 M^{11} \sim \nu\frac{K\kappa_{22}}{a^2} \sim \frac{\epsilon K}{a^3}\frac{1}{\ell^2}$
Pre-Stress and Axial Curvature		$\kappa_{22} \sim \frac{\epsilon a}{L^2}$	$N^{22}b_{22} \sim \frac{F\kappa_{22}}{2\pi a} \sim \frac{\epsilon K}{a^3}\frac{Fa}{2\pi K\ell^2}$

Table A: *Scale estimates for contributions to the normal stress balance (2.7a) induced by typical transverse displacements of $O(\epsilon a)$ and axial displacements of $O(\epsilon'_\tau a, \epsilon'_z a)$. For each mechanism, we show the incremental strain γ or curvature κ, the term through which it contributes to (2.7a), the estimate for this term in terms of γ and κ using (2.9),* (A1) and (A2). The final estimate is obtained by eliminating γ and κ and using $D \sim K/(a\delta)^2$.

$O(a\epsilon'_\tau)$ to have zero azimuthal average over each cross-section, while the displcements of $O(a\epsilon'_z)$ vary only with the axial coordiante z. The estimates of the stress components are needed in the sub-sections below, where we shall consider possible balances in (2.7) to determine ϵ, ϵ'_τ and ϵ'_z in terms of the applied pressure scale $\mathscr{P}$.

The terms in (2.7) each comprise a stress resultant $N^{\alpha\beta}$ or $M^{\alpha\beta}$, and possibly some spatial derivatives ∇_α and/or the curvature tensor $b_{\alpha\beta}$. Using the constitutive equations (2.9), the stress resultants can in turn be written in terms of the strains $\gamma_{\alpha\beta}$ and $\kappa_{\alpha\beta}$, the stretching and bending stiffnesses D and K, and the curvature $b_{\alpha\beta}$.

In tables A–C, we consider each component of the in-plane strain $\gamma_{\alpha\beta}$ or the bending strain $\kappa_{\alpha\beta}$ in turn, and estimate the size of its dominant contribution to (2.7). (The bending components are omitted from Table C since these estimates are unnecessary for the scaling arguments below.)

Derivatives are estimated using the natural length scales, so

$$\frac{\partial}{\partial x^1} \sim \frac{1}{a}, \qquad \frac{\partial}{\partial x^2} \sim \frac{1}{L}. \tag{A1a,b}$$

The scales used for the in-plane strain $\gamma_{\alpha\beta}$ and curvature $\kappa_{\alpha\beta}$ are obtained by dividing the appropriate displacement scale by the scale for the appropriate derivatives. These are shown in second column of Table A. (Note that ϵ'_z describes displacements that depends only on the axial

	Mechanism	Strain	Dominant contribution to (2.7b)
Stretching	Azimuthal	$\gamma_{11} \sim \dfrac{\epsilon a}{a}$	$\nabla_1 N^{11} \sim \dfrac{D\gamma_{11}}{a} \sim \dfrac{\epsilon K}{a^3}\dfrac{1}{\delta^2}$
	Shear	$\gamma_{12} \sim \dfrac{\epsilon a}{L}, \dfrac{\epsilon'_\tau a}{a}$	$\nabla_2 N^{21} \sim \dfrac{D\gamma_{12}}{L} \sim \dfrac{\epsilon K}{a^3}\dfrac{1}{\delta^2\ell^2}\left(1, \dfrac{\epsilon'_\tau \ell}{\epsilon}\right)$
	Axial	$\gamma_{22} \sim \dfrac{\epsilon'_\tau a}{L}, \dfrac{\epsilon'_z a}{L}$	$\nabla_1 N^{11} \sim \nu\dfrac{D\gamma_{22}}{a} \sim \dfrac{\epsilon K}{a^3}\dfrac{1}{\delta^2}\left(\dfrac{\epsilon'_\tau}{\epsilon\ell}\right)$
Bending	Azimuthal	$\kappa_{11} \sim \dfrac{\epsilon a}{a^2}$	$b^1_1\nabla_1 M^{11} \sim \dfrac{K\kappa_{11}}{a^2} \sim \dfrac{\epsilon K}{a^3}$
	Torsion	$\kappa_{12} \sim \dfrac{\epsilon a}{aL}$	$b^1_1\nabla_2 M^{21} \sim \dfrac{K\kappa_{12}}{aL} \sim \dfrac{\epsilon K}{a^3}\dfrac{1}{\ell^2}$
	Axial	$\kappa_{22} \sim \dfrac{\epsilon a}{L^2}$	$b^1_1\nabla_1 M^{11} \sim \nu\dfrac{K\kappa_{22}}{a^2} \sim \dfrac{\epsilon K}{a^3}\dfrac{1}{\ell^2}$
	Pre-Stress and Axial Curvature	$\Gamma^1_{22} \sim \dfrac{\epsilon a}{L^2}$	$\Gamma^1_{22}N^{22} \sim \dfrac{F\Gamma^1_{22}}{2\pi a} \sim \dfrac{\epsilon K}{a^3}\dfrac{Fa}{2\pi K\ell^2}$

Table B: *Scale estimates for the azimuthal stress contributions to (2.7b) induced by strains arising from typical azimuthal displacements of $O(\epsilon a)$ and axial displacements of $O(\epsilon'_\tau a, \epsilon'_z a)$. Other details as in Table A.*

coordinate z, which therefore do not contribute to terms involving an azimuthal derivative of the axial displacement, e.g. γ_{12}.)

For the curvature $b_{\alpha\beta}$, there is only one non-zero component in the undeformed configuration, namely $\bar{b}_{11} \sim a^{-1}$. Using (2.8b), the leading-order curvature scales are therefore given by

$$b_{11} \sim \frac{1}{a}, \qquad b_{12} \sim \kappa_{12}, \qquad b_{22} \sim \kappa_{22}, \tag{A2a–c}$$

where the scales for $\kappa_{\alpha\beta}$ can be found in Table A.

The estimates in tables A–C come from scaling arguments based on derivatives not vanishing and terms not cancelling. It is quite possible (and indeed will turn out to be the case) that some of the quantities will be smaller than their estimates, due to the form of the deformations. For example, if the tube deforms in such a way that there is almost no azimuthal stretching, then the strain γ_{11} will be smaller than its estimate.

A.2 *Determining the leading-order balances and the size of the hoop stress N^{11}*

The size of the deformations induced by transmural pressures of size $\mathscr{P}$ is determined by the requirement that the deformations are able to provide a normal force of the appropriate magnitude and spatial distribution to balance the pressure, and that the tangential and axial forces from the shell are in balance. We now consider the possible leading-order balances in each direction using the estimates in tables A–C.

The deformations of the tube are forced by the transmural pressure, so the pressure should be

	Mechanism	Strain	Dominant contribution to (2.7c)
Stretching	Azimuthal	$\gamma_{11} \sim \dfrac{\epsilon a}{a}$	$\nabla_2 N^{22} \sim \nu \dfrac{D\gamma_{11}}{L} \sim \dfrac{\epsilon K}{a^3}\dfrac{1}{\delta^2\ell}$
	Shear	$\gamma_{12} \sim \dfrac{\epsilon a}{L}, \dfrac{\epsilon'_\tau a}{a}$	$\nabla_1 N^{12} \sim \dfrac{D\gamma_{12}}{a} \sim \dfrac{\epsilon K}{a^3}\dfrac{1}{\delta^2\ell}\left(1, \dfrac{\epsilon'_\tau \ell}{\epsilon}\right)$
	Axial	$\gamma_{22} \sim \dfrac{\epsilon'_\tau a}{L}, \dfrac{\epsilon'_z a}{L}$	$\nabla_2 N^{22} \sim \dfrac{D\gamma_{22}}{L} \sim \dfrac{\epsilon K}{a^3}\dfrac{1}{\delta^2\ell}\left(\dfrac{\epsilon'_\tau}{\epsilon\ell}, \dfrac{\epsilon'_z}{\epsilon\ell}\right)$

Table C: *Scale estimates for the axial stress contributions to (2.7c) induced by strains arising from typical azimuthal displacements of $O(\epsilon a)$ and axial displacements of $O(\epsilon'_\tau a, \epsilon'_z a)$. Other details as in Table A. The curvature components are omitted here, since they are higher-order effects, which we do not need to consider in detail here.*

present in the dominant normal force balance. We shall also choose the axial tension F so that axial curvature effects are present at leading order. We begin our analysis by assuming, on geometric grounds, that $\epsilon'_\tau, \epsilon'_z \ll \epsilon$ — in other words that the physical displacements in the axial direction are much smaller than those in the normal or transverse directions.

Considering the axial force balance (Table C) we see that we must have $\epsilon'_\tau \leq \epsilon/\ell$ or else the contribution to the shear would be larger than any of the other terms. We can then observe, from the normal force balance (Table A), that if the hoop stress N^{11} is azimuthally uniform it cannot balance the azimuthally uniform pressure in isolation, as the curvature b_{11} is not azimuthally uniform.

Examining the azimuthal force balance (Table B), we see that based on the scaling arguments, the term arising from azimuthal stretching dominates. By virtue of the ∇_1 derivative, the strain γ_{11} and hoop stress N^{11} are therefore azimuthally uniform at leading order. Any component exhibiting azimuthal variation must be small enough to balance another term in table B, the largest of which are the shear, axial stretching or azimuthal bending. Components of N^{11} with azimuthal variation must therefore be at least $O(\delta^2, \ell^{-2})$ smaller than the scale given.

Returning to Table A, if the hoop stress is to be present in the leading-order balance with the pressure, it must be smaller than its natural estimate — either to allow azimuthal variation, or to allow additional terms to contribute to the normal force balance. We have seen above that azimuthal variation requires N^{11} to be $O(\delta^2, \ell^{-2})$ smaller than its natural estimate. The next largest term in the normal force balance arises from azimuthal bending, and so this would require N^{11} to be $O(\delta^2)$ smaller.

If $\delta^2\ell^2 \gtrsim 1$ then both possibilities occur first when N^{11} is $O(\delta^2)$ smaller than its natural estimate. We therefore have $N^{11} = O(\epsilon K/a^2)$.

If $\delta^2\ell^2 \ll 1$ then the situation is more complicated. We could potentially take N^{11} to be $O(\ell^{-2})$ smaller than its natural estimate, thus allowing azimuthal variation (via the azimuthal force balance in Table B) without introducing any more terms into the normal force balance (in Table A). Then $N^{11} = O(\epsilon K/(a^3\delta^2\ell^2))$ which allows a balance with the shear term in Table B). However, from the axial force balance (Table C) if γ_{11} is smaller than its natural estimate, then so too is the shear term there (for there is nothing else with which it can balance at $O(\epsilon K/(a^3\delta^2\ell))$). Then, by virtue of the ∇_1 derivative, $N^{21} \approx N^{12}$ is uniform in the azimuthal coordinate at leading order.

Returning to Table B, we then have that $\nabla_1 N^{11}$ is constant, and so N^{11} can only vary linearly in the azimuthal coordinate. Periodicity implies that N^{11} must still be uniform. Therefore a balance with N^{11} being only $O(\ell^{-2})$ smaller is not possible, and we must again take $N^{11} = O(\epsilon K/a^2)$.

A.3 *The axial force balance (Table C)*

In the leading-order axial force balance, we need to include all three of the stretching terms. We first consider an average over the azimuthal coordinate, in order to eliminate the shear effects. The resulting balance involves just the axial stress N^{22}, with contributions from azimuthal and axial stretching. Hence the azimuthal average of N^{22} must vanish at its anticipated order. To leading order, the axial stress can be expressed as

$$N^{22} = \nu N^{11} + (1-\nu^2) D \gamma_{22} \,. \tag{A3}$$

The size of the azimuthally averaged axial strain γ_{22} is therefore determined by the hoop stress $N^{11} = O(\epsilon K/a^2)$. Comparing with the scale estimate for γ_{22}, and noting that ϵ'_τ does not contribute to the azimuthal average, we find that

$$\epsilon'_z = \epsilon \delta^2 \ell \,. \tag{A4}$$

Considering the full axial stress balance, we see (from (A3) and the estimates for N^{11} and γ_{22}) that the revised estimate for the axial and azimuthal stretching terms involving N^{22} is now

$$\nabla_2 N^{22} \lesssim \frac{\epsilon K}{a^3} \frac{1}{\delta^2 \ell} \max\{\delta^2, \ell^{-2}\} \tag{A5}$$

The estimate for shear term in Table C is larger than this, and so its two components must cancel between themselves at leading order. The means we must take

$$\epsilon'_\tau \sim \frac{\epsilon}{\ell} \,, \tag{A6}$$

and then we must have

$$\nabla_1 \gamma_{12} \lesssim \frac{\epsilon}{a\ell} \max\bigl\{\delta^2, \ell^{-2}\bigr\} \,. \tag{A7}$$

This is a factor $\max\bigl\{\delta^2, \ell^{-2}\bigr\}$ smaller than one would expect from general displacements of size ϵ, so this condition means the tube deforms with negligible shearing.

With the scales for ϵ'_τ and ϵ'_z above, we have that the axial strain scales as

$$\gamma_{22} \sim \epsilon \ell \max\{\delta^2, \ell^{-2}\} \,. \tag{A8}$$

This does not represent a constraint on the axial stretching.

A.4 *The normal force balance (Table A)*

The leading-order normal force balance comprises the hoop stress (azimuthal and axial stretching), azimuthal bending, all of size $O(\epsilon K/a^2)$; to balance the applied pressure, of size $O(\mathscr{P})$. We also want the axial curvature effects, of $O(\epsilon K/a^2 \tilde{F})$, to enter at the same order. Comparing the magnitudes, we must therefore take

$$\epsilon = \frac{a^3 \mathscr{P}}{K} \,, \qquad \tilde{F} \equiv \frac{aF}{2\pi K \ell^2} = O(1) \,, \tag{A9a,b}$$

which determines the size of the deformations and the required strength of the axial pre-stress.

The deformations must be such that the hoop stress N^{11} is $O(\delta^2)$ smaller than its natural estimate. Given the scale (A8) for the axial strain, this requires the azimuthal strain to be constrained by

$$\gamma_{11} \lesssim \epsilon \max\bigl\{\delta^2, \ell^{-2}\bigr\} \,. \tag{A10}$$

This is a factor $\max\bigl\{\delta^2, \ell^{-2}\bigr\}$ smaller than one would expect from general displacements of size ϵ, so this condition means the tube deforms with negligible azimuthal stretching.

A.5 *The azimuthal force balance (Table B)*

In the leading-order azimuthal force balance, we have the hoop stress (azimuthal and axial stretching), azimuthal bending, and axial curvature, all of size $O(\epsilon K/a^2)$. We also have the in-plane shear with size $O(\epsilon K/(a^2\delta^2\ell^2))$. If $\delta^2\ell^2 \ll 1$ we therefore have a constraint on the deformations to prevent the shear from being too large. In this case, we require

$$\nabla_2\gamma_{12} \lesssim \frac{\epsilon}{\ell^2}\,\delta^2\ell^2\,. \tag{A11}$$

APPENDIX B

Curvature and in-plane strain components in terms of the deformation functions

In this appendix, we obtain expressions for the four dimensionless curvatures $(\overline{B}, \beta, \mathbb{B}_{\rm n}, \mathbb{B}_{\rm t})$ in terms of the deformation functions (ξ, η, ζ). We also analyse the constraints on the displacements that arise from (2.11a) and (2.11b).

In the undeformed state, the basis vectors are given by

$$\bar{\boldsymbol{a}}_1 \equiv \frac{\partial\bar{\boldsymbol{r}}}{\partial x^1} = \hat{\boldsymbol{t}}\,, \qquad \bar{\boldsymbol{a}}_2 \equiv \frac{\partial\bar{\boldsymbol{r}}}{\partial x^2} = \hat{\boldsymbol{z}}\,, \qquad \bar{\boldsymbol{a}}_3 = \frac{\bar{\boldsymbol{a}}_1\times\bar{\boldsymbol{a}}_2}{|\bar{\boldsymbol{a}}_1\times\bar{\boldsymbol{a}}_2|} = \hat{\boldsymbol{n}}\,. \tag{B1a–c}$$

The curvatures are defined by

$$\bar{b}_{\alpha\beta} = \bar{\boldsymbol{a}}_3\cdot\frac{\partial\bar{\boldsymbol{a}}_\alpha}{\partial x^\beta}\,, \tag{B2}$$

so the dimensionless azimuthal curvature $\overline{B} \equiv a\bar{b}_{11}$ in the undeformed state is given by

$$\overline{B} = \hat{\boldsymbol{n}}\cdot\frac{1}{h}\frac{\partial\hat{\boldsymbol{t}}}{\partial\tau} = -\frac{c^2\sinh 2\sigma_0}{2h^3} \tag{B3}$$

The other components of $\bar{b}_{\alpha\beta}$ are zero.

Using the deformations defined in (2.19), we find that

$$\boldsymbol{a}_1 = \hat{\boldsymbol{t}} + \frac{\epsilon}{h}\left[\left(-\xi\overline{B} + \frac{\partial}{\partial\tau}\left(\frac{\eta}{h}\right)\right)\hat{\boldsymbol{t}} + \left(\eta\overline{B} + \frac{\partial}{\partial\tau}\left(\frac{\xi}{h}\right)\right)\hat{\boldsymbol{n}} + \frac{1}{\ell}\frac{\partial\zeta}{\partial\tau}\hat{\boldsymbol{z}}\right]\,, \tag{B4a}$$

$$\boldsymbol{a}_2 = \hat{\boldsymbol{z}} + \frac{\epsilon}{h\ell}\left(\frac{\partial\xi}{\partial z}\hat{\boldsymbol{n}} + \frac{\partial\eta}{\partial z}\hat{\boldsymbol{t}}\right) + \epsilon\left(\frac{1}{\ell^2}\frac{\partial\zeta}{\partial z} + \delta^2\frac{\mathrm{d}\zeta_a}{\mathrm{d}z}\right)\hat{\boldsymbol{z}}\,, \tag{B4b}$$

$$\boldsymbol{a}_3 = \hat{\boldsymbol{n}} + \frac{\epsilon}{h}\left[\left(\eta\overline{B} + \frac{\partial}{\partial\tau}\left(\frac{\xi}{h}\right)\right)\hat{\boldsymbol{t}} - \frac{1}{\ell}\frac{\partial\xi}{\partial z}\hat{\boldsymbol{z}}\right] + O(\epsilon^2)\,. \tag{B4c}$$

From (2.11a) and (2.11b) we see that some of the components of $\gamma_{\alpha\beta}$ are restricted. By substituting (B4) into (2.8a), we find that at leading order

$$-\xi\overline{B} + \frac{\partial}{\partial\tau}\left(\frac{\eta}{h}\right) = 0\,, \tag{B5a}$$

$$\frac{\partial\eta}{\partial z} + \frac{\partial\zeta}{\partial\tau} = h(\tau)\,s(z)\,, \tag{B5b}$$

where $s(z)$ is introduced as a constant of integration. There are no particular constraints on the axial stretching, since the scales for ϵ'_τ and ϵ'_z already force it to be small. Equation (B5a) implies there is no azimuthal stretching at leading order, and provides a constraint on ξ and η. Equation (B5b) imposes a constraint on the form of the shearing at leading order. Since ζ must be periodic in τ, integrating (B5b) with respect to τ yields

$$s(z) = \frac{\mathrm{d}}{\mathrm{d}z}\left(\frac{1}{2\pi}\int_0^{2\pi}\eta\,\mathrm{d}\tau\right)\,. \tag{B6}$$

Equation (B5b), combined with (2.20) allows ζ to be recovered from $\eta(\tau, z)$.

Using (B4a), (B4c) and (B5a), the azimuthal curvature is found to be given by

$$b_{11} \equiv \boldsymbol{a}_3 \cdot \frac{\partial \boldsymbol{a}_1}{\partial x^1} = \frac{1}{a}\left(\overline{B} + \frac{\epsilon}{h}\beta + O(\epsilon^2)\right), \tag{B7}$$

where we have introduced

$$\beta = \frac{\partial}{\partial \tau}\left[\frac{\eta \overline{B}}{h} + \frac{1}{h}\frac{\partial}{\partial \tau}\left(\frac{\xi}{h}\right)\right]. \tag{B8}$$

The inextensibility condition (B5a) may be rewritten as

$$\xi \sinh 2\sigma_0 + \frac{2h^2}{c^2}\frac{\partial \eta}{\partial \tau} - \eta \sin 2\tau = 0\,, \tag{B9}$$

and the expression (B8) for the curvature perturbation as

$$\beta = -\frac{\partial}{\partial \tau}\left[\frac{c^2}{2h^4}\left(\eta \sinh 2\sigma_0 - \frac{2h^2}{c^2}\frac{\partial \xi}{\partial \tau} + \xi \sin 2\tau\right)\right]. \tag{B10}$$

Then, eliminating ξ between (B9) and (B10), we obtain

$$\beta(\tau) = \frac{-2}{c^2 \sinh 2\sigma_0}\frac{\partial}{\partial \tau}\left(1 + \frac{\partial^2}{\partial \tau^2}\right)\eta\,. \tag{B11}$$

Using (B4b) and (B4c), the axial curvature is given by

$$b_{22} \equiv \boldsymbol{a}_3 \cdot \frac{\partial \boldsymbol{a}_2}{\partial x^2} = \frac{\epsilon \delta^2}{a\lambda^2 h}\mathbb{B}_{\rm n}\,, \qquad \text{where} \qquad \mathbb{B}_{\rm n} = \frac{\partial^2 \xi}{\partial z^2}\,. \tag{B12a,b}$$

Finally, using (B4a) and (B4b), the Christoffel symbol in the derivative is given by

$$\Gamma^1{}_{22} = \boldsymbol{a}^1 \cdot \frac{\partial \boldsymbol{a}_2}{\partial x^2} = \frac{\epsilon \delta^2}{a\lambda^2 h}\mathbb{B}_{\rm t}\,, \qquad \text{where} \qquad \mathbb{B}_{\rm t} = \frac{\partial^2 \eta}{\partial z^2}\,. \tag{B13a,b}$$

APPENDIX C

Elastic energy and solution symmetries

In this appendix, we derive an expression for the elastic energy stored in a deformed configuration, and use this to show that the solutions to (3.19) subject to periodic boundary conditions in τ and $\xi = \eta = 0$ at $z = 0, 1$ must have certain symmetries.

The elastic energy is a function of the geometry of the deformed tube, and the deformation is linear in the transmural pressure. The energy is therefore equal to the work done by the pressure while moving from the undeformed state to the deformed state. The dimensionless elastic energy is therefore

$$E = \frac{1}{2}\int_0^1 \int_0^{2\pi} \xi(\tau, z)\tilde{P}(z)\,\mathrm{d}\tau\,\mathrm{d}z\,. \tag{C1}$$

Using (B5a) to eliminate ξ, and then integrating by parts, we obtain

$$E = \frac{1}{2}\int_0^1 \int_0^{2\pi} \eta\, C_P \tilde{P}\,\mathrm{d}\tau\,\mathrm{d}z\,. \tag{C2}$$

Substituting for $C_P\tilde{P}$ from the governing equation (3.19), we then obtain

$$E = \frac{1}{2}\int_0^1 \int_0^{2\pi} \frac{\eta}{h}\left\{\mathscr{L}(\beta) - h\frac{\partial^2}{\partial z^2}\mathscr{I}(\eta) - \tilde{F}\frac{\partial^2}{\partial z^2}\mathscr{J}(\eta)\right\}\mathrm{d}\tau\,\mathrm{d}z\,. \tag{C3}$$

Finally, using further integration by parts, together with (B5a) and (B8), we arrive at

$$E = \frac{1}{2}\int_0^1 \int_0^{2\pi} \frac{1}{h}\left\{\beta^2 + \tilde{F}\left[\left(\frac{\partial \xi}{\partial z}\right)^2 + \left(\frac{\partial \eta}{\partial z}\right)^2\right] + \frac{12(1-\nu)(hs)^2}{\ell^2\delta^2}\right\} \mathrm{d}\tau\,\mathrm{d}z\,. \tag{C4}$$

As the expression (C4) for E is positive definite in ξ_z, η_z, β, and s it follows that when $\tilde{P} = 0$, the only solution to the governing equation with the homogeneous boundary conditions specified above is the zero solution.

Now suppose that $\eta_1(\tau, z)$ and $\eta_2(\tau, z)$ are solutions of (3.19) with homogeneous boundary conditions and transmural pressure $\tilde{P}(z)$. The using the linearity of the operators $\mathscr{L}$, $\mathscr{K}$, $\mathscr{I}$, and $\mathscr{J}$ it can be shown that

$$\tilde{\eta} = \eta_1(\tau, z) - \eta_2(\tau, z) \tag{C5}$$

satisfies (3.19) with $\tilde{P}(z) \equiv 0$. Therefore $\tilde{\eta} = 0$, and the solution to the original problem is unique.

Similarly, for any solution $\eta(\tau, z)$ the linearity and symmetries implies that both

$$\hat{\eta} \equiv \eta(\tau, z) - \eta(-\tau, z) \qquad \text{and} \qquad \breve{\eta} \equiv \eta(\tau, z) - \eta(\tau + \pi, z)\,, \tag{C6a,b}$$

satisfy (3.19) with $\tilde{P}(z) \equiv 0$. Therefore $\hat{\eta} = \breve{\eta} = 0$, and the solution $\eta(\tau, z)$ must be odd and π-periodic in τ.